AD_____

Award Number: W81XWH-12-1-0604

TITLE: Deciphering the Adaptive Immune Response to Ovarian Cancer

PRINCIPAL INVESTIGATOR:

Brad H. Nelson, Ph.D.

CONTRACTING ORGANIZATION:

British Columbia Cancer Agency,
Victoria BC V8R 6V5
Canada

REPORT DATE:

December 2015

TYPE OF REPORT:

Final

PREPARED FOR: U.S. Army Medical Research and Materiel Command
Fort Detrick, Maryland 21702-5012

REPORT DOCUMENTATION PAGE

Form Approved
OMB No. 0704-0188

1. REPORT DATE *(DD-MM-YYYY)*	2. REPORT TYPE	3. DATES COVERED *(From - To)*
December 2015	Final Report	30 Sep 2012 - 29 Sep 2015

4. TITLE AND SUBTITLE
Deciphering the Adaptive Immune Response to Ovarian Cancer

5a. CONTRACT NUMBER

5b. GRANT NUMBER
W81XWH-12-1-0604

5c. PROGRAM ELEMENT NUMBER

6. AUTHOR(S)
Brad H. Nelson, Ph.D.

5d. PROJECT NUMBER

5e. TASK NUMBER

5f. WORK UNIT NUMBER

7. PERFORMING ORGANIZATION NAME(S) AND ADDRESS(ES)

British Columbia Cancer
Agency,
2410 Lee Avenue,
Victoria BC V8R 6V5
Canada

8. PERFORMING ORGANIZATION REPORT NUMBER

9. SPONSORING / MONITORING AGENCY NAME(S) AND ADDRESS(ES)
US Army Medical Research and
Material Command
Fort Detrick, Maryland
21702-5012

10. SPONSOR/MONITOR'S ACRONYM(S)

11. SPONSOR/MONITOR'S REPORT NUMBER(S)

12. DISTRIBUTION / AVAILABILITY STATEMENT
Approved for public release; distribution unlimited

13. SUPPLEMENTARY NOTES

14. ABSTRACT The presence of CD8+ tumor-infiltrating lymphocytes (CD8+ TIL) has been associated with increased patient survival in ovarian cancer. We discovered that this effect is even stronger when CD8+ TIL are found together with CD20+ B cells and CD4+FoxP3+ T cells. We hypothesized that CD20+ TIL contribute to tumor immunity by presenting antigens to CD4+ and CD8+ TIL. During the funding period, we discovered that the major antibody-producing cells in ovarian cancer are not CD20+ TIL but plasma cells, therefore our immunoglobulin cloning efforts have been directed toward these cells. We also discovered an unexpectedly high diversity of T cell receptors (TCR) among tumor-infiltrating T cells, which prompted us to develop a new high throughput method for T cell antigen discovery. Finally, we discovered a novel subset of CD4+ T cells that is strongly associated with patient survival and will be the focus of future antigen identification efforts. Overall, this project progressed on schedule and yielded innovative methods, multiple publications, and new funding sources, all of which will faciliate the development of more effective immunotherapies for ovarian cancer.

15. SUBJECT TERMS
Tumor immunology, immunotherapy, ovarian cancer, antibody, T cell, tumor antigen

16. SECURITY CLASSIFICATION OF:			17. LIMITATION OF ABSTRACT	18. NUMBER OF PAGES	19a. NAME OF RESPONSIBLE PERSON
a. REPORT	b. ABSTRACT	c. THIS PAGE			USAMRMC
U	U	U	UU	16	19b. TELEPHONE NUMBER *(include area code)*

Table of Contents

W81XWH-12-1-0604 (OC110435) Final Report, Dec 2015

PI: Brad H. Nelson, Ph.D.
Co-PIs: Rob Holt, Ph.D., John Webb Ph.D., Peter Watson, M.D.

Title of Project: Deciphering the Adaptive Immune Response to Ovarian Cancer

INTRODUCTION:

Tumor-infiltrating CD8+ T cells (CD8+ TIL) are strongly associated with increased survival in ovarian cancer. However, they do not work in isolation. Prior to our DOD Teal Award, we discovered that two other types of immune cell play an important supportive role: B cells and helper T cells. We made this discovery by performing a systematic analysis of immune cells in ovarian cancer. We found that killer T cells are often found in small clusters together with B cells and helper T cells. Importantly, we found that patients whose tumors have these combinations of immune cells have better survival rates than patients whose tumors contain killer T cells alone **(Figure 1)**. This tells us that T cells and B cells work together to attack tumors. These findings have powerful clinical implications: to enhance the immune response to ovarian cancer, we need to enhance the activity of all three types of immune cell, rather than killer T cells alone.

To explain these observations, we hypothesized that B cells serve as "organizers" that help to draw T cells into the tumor. In addition, we reasoned that B cells might present tumor proteins to the T cells to facilitate tumor recognition. We further hypothesized that helper T cells might produce cytokines that help to stimulate the killer T cells. To test these hypotheses, in our Teal Award we proposed to determine which tumor proteins (antigens) are recognized by B cells and helper T cells in high-grade serous ovarian cancer (HGSC). By identifying these antigens, we would create new molecular tools to elucidate how the immune system recognizes and attacks ovarian cancer. The study had four tasks:

Task 1. To identify tumor antigens recognized by CD20+ TIL.

Task 2. To identify tumor antigens recognized by CD4+FoxP3+ TIL.

Task 3. To determine whether tumor-infiltrating B cells and T cells recognize the same antigens.

Task 4. To assess the functional phenotype of antigen-specific CD4+FoxP3+ TIL.

Significance: The immune system has a profound influence on survival from ovarian cancer. With better understanding of the immune response, it will be possible to design new treatments such as vaccines and adoptive T cell therapies that enhance tumor immunity and increase patient survival. We envisioned our work would lead to a major re-think about cancer vaccines: instead of simply trying to activate killer T cells, we also need to find effective ways to activate their team mates, the B cells and helper T cells.

BODY:

Task 1. To identify tumor antigens recognized by CD20+ TIL.

In this task, we proposed to identify the antigens recognized by the 3 most abundant CD20+ TIL clones from each of 3 ovarian cancer patients. To accomplish this, we proposed to clone immunoglobulin G (IgG) molecules from individual CD20+ TIL. These would be used to identify the corresponding antigens using three different approaches: candidate antigen assays, cDNA library screening, and mass spectrometry.

Progress:

1.1 Generating IgG and TCR profiles from ovarian tumor specimens

To identify the 3 most abundant IgG (for Task 1) and TCR clones (for Task 2) in each patient's tumor, we used deep sequencing methods developed in the Holt lab. Our approach for deep sequence analysis of T cell receptor (TCR) beta chain diversity has been previously described (1, 2), and we made adaptations to enable B cell receptor (BCR) heavy chain profiling and sample multiplexing, as described below. We isolated total RNA from bulk ascites from the three HGSC ovarian cancer study subjects at three different timepoints (the time of primary disease, at first recurrence, and at second recurrence). First strand cDNA was synthesized from total RNA using either TCR beta chain or BCR heavy chain gene-specific primers, and this cDNA was then used as template to amplify the CDR3 sequences from each receptor population by PCR. The CDR3 region is the site of VDJ recombination and is the most highly variable and thus most informative region for the purpose of profiling repertoire diversity. The PCR primers were tagged with unique, 6 base pair, error tolerant barcode sequences. A different barcode was used for each individual sample. The CDR3 amplicons were then subjected to several additional rounds of nested PCR using primers tailed with Illumina adapter sequences necessary for annealing to the Illumina flow cell surface for massively parallel sequencing. The samples were pooled and sequenced using a single flow cell and the Illumina miSeq platform. Sequence data was then de-convoluted based on the barcode identifiers, and the TCR and BCR CDR3 sequences were filtered to remove low quality reads, then clustered using standard bioinformatic methods. Clustering was done to determine the number of distinct CDR3 sequences present in each sample, which reflects the diversity of distinct T-cell and B-cell clonotypes with the original ascites specimens. Prior to reverse transcription and PCR each sample was spiked with RNA from a single, known clonotype in order to monitor PCR and sequence error rates and the efficiency of sequence recovery.

We filtered and analyzed the sequence data derived from specimens taken from each of the three timepoints for one of the three study subjects. We obtained over 30,000 total TCR beta chain CDR3 sequences from each of these three samples, and over 15,000 total BCR heavy chain CDR3 sequences from each of these same three samples. These collapsed, upon clustering, into a much smaller number of distinct sequences. Specifically there were 1,598 distinct TCR sequences and 688 distinct BCR sequences observed per sample. However, as expected, the majority of these unique sequences were "singletons", representing rare clonotypes, with the bulk of the accumulated sequence data from each sample represented approximately 30 clonotypes per sample. Thus the ascites repertories are polyclonal, but not to the same extent as peripheral blood, where previously we have been able to detect over a million distinct sequences from a single sample by deep sequencing. Interestingly, 18 of the BCR clonotypes were detectable at all three timepoints, albeit with varying abundance, but the TCR clonotypes were much more sample specific, with only one TCR clonotype being present in all three samples.

1.2 Amplification of matched IgG heavy and light chains by single-cell RT-PCR

Single cell sorting and PCR amplification of matched immunoglobulin (Ig) heavy and light chains from tumor-infiltrating B lymphocytes was accomplished using methods similar to Tiller et al. (3). Single B cells were isolated based on their surface expression of CD19, CD20 and IgG using a BD Influx cell sorter. Individual cells were sorted directly into single wells of 96-well PCR plates. Reverse transcription was accomplished directly within the sorting plate, which yielded cDNA corresponding to the original single cell. This cDNA was then split equally between four separate PCR reactions, one each for the variable portions of Ig heavy, kappa, and lambda, and one for the control housekeeping gene GAPDH. The variable portions of the

immunoglobulin genes were then amplified by sequential nested multiplex PCR using primer sets known to amplify all human variable and joining gene segments and containing restriction enzyme cut sites to facilitate downstream molecular cloning. We successfully amplified matched pairs of Ig genes from B cells isolated from the tumors of three high-grade serous ovarian cancer patients. Roughly 70% of all sorting wells yield amplification of at least one B cell-specific gene product, while about 10-25% yield matched pairs of heavy and light chains. In total, we successfully amplified over 30 pairs of Ig genes from the 3 patients.

1.3 Cloning of CDR3 regions into IgG expression vectors

Molecular cloning of the PCR amplified variable portions of matched heavy and light chain genes derived from single sorted tumor infiltrating B cells was accomplished by standard techniques. All amplified pairs were subsequently cloned into appropriate expression vectors containing the signal sequence and constant portions of the corresponding germline immunoglobulin chain (heavy, kappa, lambda). Once inserted into these expression vectors, the DNA sequence of each immunoglobulin chain was determined by Sanger sequencing. Sequences for each of the pairs of heavy and light chains were obtained. We evaluated the prevalence of each immunoglobulin heavy sequence by sequencing samples prepared by conventional RT-PCR of bulk tumor preparations.

1.4 Preparation of recombinant IgG (rIgG)

To produce recombinant IgG, two expression vectors encoding cloned matched heavy and light chain variable portions were co-transfected into log-phase 293T cells. This transient transfection was accomplished by a calcium phosphate precipitation method. After seven days in culture, supernatants were harvested and assessed for the presence of rIgG by human IgG-specific western blot. Fully assembled IgG molecules (~150 kDa) were observed in the supernatant of 80-90% of culture transfected with different pairs of expression vectors under non-reducing conditions. To isolate rIgG from the culture supernatant, it was concentrated and run over protein G sepharose columns. Captured IgG molecules were eluted at low pH and the resulting eluate was neutralized and desalted. Further concentration and assessment of purity was accomplished by BCA assay and additional western blot analysis. Over 30 recombinant antibodies were successfully expressed in vitro, for an overall success rate of 80%.

1.5 Discovery of plasma cells as the major source of IgG in HGSC

Unexpectedly, none of the IgG sequences from the above CD20+ B cells aligned to the dominant clonotypes determined by sequencing of bulk tumor tissue. Furthermore, on screening recombinant antibodies against HGSC cell lines, we obtained no evidence of tumor reactivity. This puzzling result led us to hypothesize that the B cell component of TIL might be more heterogeneous than previously appreciated. We therefore turned to immunohistochemistry and flow cytometry to further investigate B-lineage cells in HGSC.

To this end, we performed multicolor immunohistochemistry on whole tumor sections from 21 HGSC patients. We found that CD20+ B cells often form dense aggregates with other lymphocytes within and around HGSC tumors **(Figures 2 and 3)**. These aggregates resemble lymph nodes, yet are embedded within tumor tissue. Others have named these “ectopic lymphoid follicles” or “tertiary lymphoid structures” (TLS); we will use the latter designation. TLS appear to have all the components of normal lymph nodes. They have T cell zones containing CD4+ and CD8+T cells; activated dendritic cells expressing CD208; and high endothelial venules (HEVs). They also contain B cell-rich areas (called follicles), which contain interdigitating networks of follicular DCs, follicular helper T cells and germinal center B cells **(Figure 3)**. We found the latter cells express the transcription factor Bcl-6 and activation-induced cytidine deaminase (AID), an enzyme involved in class-switch recombination and

somatic hypermutation. Thus, TLS resemble lymph nodes in their organization, cellular composition, and ability to support immune reactions.

By flow cytometry, we found that the vast majority of tumor-infiltrating CD20+ B cells are IgG+ memory B cells **(Figure 4)**. Most of these memory B cells appear to be activated (i.e., they express FAS) and express IgG. However, we also discovered that 9/10 cases contained an appreciable number of early plasma cells ($CD38^{high}$, $CD138^{low}$, IgD-) **(Figure 4)**. The proportion of these cells ranged from <5% to >80% of CD19+ cells. Importantly, these plasma cells do not express CD20 and therefore have been missed in previous immunohistochemical and sorting experiments **(Figure 5)**. Plasma cells are known to express large amounts of IgG-encoding mRNA and protein. In fact, they are often referred to ask "antibody factories". Given this, we hypothesized that IgG sequencing from bulk tumor preparations might largely reflect the IgG repertoire of plasma cells. To address this, we used conventional FACS to isolate CD20+ TIL and $CD38^{high}$ plasma cells from tumor samples. We then sequenced the IgG repertoire in each sample and compared these sequences to those found in bulk tumor preparations from the same tumor **(Figure 6)**. In 3/3 patients, we found that both CD20+ TIL and $CD38^{high}$ plasma cells were clonally expanded to some extent. We also found examples of shared IgG sequences between these two populations, suggesting that some CD20+ TIL are products of the same immune reactions that give rise to plasma cells. Importantly, we found that IgG sequences derived from plasma cells were highly over-represented in sequencing data from bulk tumor **(Figure 6)**. Thus, we concluded that plasma cells in HGSC are the major source of clonally expanded IgG sequence and therefore are the more likely B lineage cell type to mediate anti-tumor immune reactions.

A manuscript describing the above findings is under review at the AACR journal *Clinical Cancer Research* **(Appendix A)**.

1.6 Cloning and production of recombinant IgG from tumor-derived plasma cells

Having identified plasma cells as the major source clonally expanded B cell populations in HGSC, we investigated the possibility that these cells are making antibodies to tumor-associated antigens. As per the original proposal, we used single-cell sorting followed by RT-PCR to molecularly clone matched IgG heavy and light chains from these cells. We isolated and PCR-cloned 15 matched IgG heavy and light chain pairs from plasma cells from an HGSC patient **(Figure 6)**. As expected, some of these antibodies correspond to clonally expanded populations dominating the IgG repertoire in both the plasma cell component and the bulk tumor **(Figures 6 and 7)**. We expressed these cloned heavy and light chains as recombinant antibodies (n=15) **(Figure 6)**.

1.7 Current work: Identifying the antigens recognized by plasma cell-derived IgG

With 15 recombinant antibodies in hand, and an efficient pipeline for producing more, we are in a strong postion to identify the underlying tumor antigens. Unfortunately, we did not reach this milestone during the funding period of this grant. However, we are actively pursuing this goal using two new sources of leveraged funding:

(a) With a new operating grant from the Canadian Institutes of Health Research (CIHR) **(see Leveraged Funding)**, we are using an innovative protein array-based approach to antigen identification. Specifically, our approach is to screen microarrays spotted with approximately 9,000 cancer- and non-cancer-associated proteins (ProtoArray, Life Technologies), as others have done in other cancers and autoimmune conditions (90-92). Importantly, the ProtoArray includes cell surface proteins (e.g., ErbB2) that have been shown to be recognized by serum antibodies from ovarian cancer patients (93). Protein arrays will be pre-blocked and probed with diluted rIgG. Bound rIgG will be detected with AlexaFluor647-conjugated anti-human IgG

secondary antibody. Arrays will be scanned using our LI-COR Odyssey, and immunoreactive antigens will be identified using ProtoArray Prospector v5.2. Key results will be validated by ELISA using recombinant antigens (Bacpower™ service; Genscript).

(b) With a new pilot grant from Canada's Networks of Centres of Excellence (NCE) program, we are collaborating with Dr. John Babcook at the Centre for Drug Research and Development (CDRD) at the University of British Columbia in Vancouver. Dr. Babcook is an international expert in antibody production and engineering. He is using mass spectrometry-based approaches (proteomics) to identify the antigens recognized by the 15 plasma cell-derived antibodies described above.

Thus, we remain committed to the goal of identifying the tumor antigens recognized by tumor-associated plasma cells in HGSC. Based on the strength of the data generated by our DOD Teal Award, we have been successful at obtaining continued funding for this challenging but important objective.

Task 2. To identify tumor antigens recognized by CD4+FoxP3+ TIL.

We proposed to clone TCR molecules from CD4+FoxP3+ tumor-infiltrating T cells from the 3 ovarian cancer patients described above. Cloned TCR's were to be expressed in a hybridoma cell line, which in turn would be used to identify the underlying antigens using a candidate approach and/or cDNA library screening.

Progress:

2.1 Discovery of extensive clonal diversity among tumor-infiltrating T cells

For Task 2, we originally proposed to choose from ascites from each of 3 patients with EOC (i.e., high-grade serous ovarian cancer), the 3 most abundant and persistent CD4+FoxP3+ TIL clones as identified by TCR-seq analysis, and proceed to identify their cognate antigens. TCR-seq analysis was completed but gave the surprising result that ascites T-cells were highly heterogeneous and we did not find any examples of abundant, persistent T-cell clones that were present in all three samples from a given subject. If we had observed a small number of dominant clontypes it would have made sense to proceed with conventional cloning and antigen identification as described in our original proposal. Now, however, we are faced with high clonal diversity of tumor associated T cells and the question of what antigens these populations of T cells are recognizing remains. This prompted us to refocus our approach, and work towards developing a more powerful, high-throughput and unbiased method for T cell antigen discovery.

2.2 Development of a novel high throughput screen to identify antigens recognized by T cells

As we have discussed in recent review articles, it is well recognized that TCR-seq has opened a new window on T-cell repertoires, but T-cell antigen profiling capabilities have not kept pace. The difficulties associated with scaling T-cell antigen profiling stem from the enormous complexity of the pMHC/TCR interaction. This complexity is generated by differential peptide processing in antigen-presenting cells, MHC allelic variation, somatic recombination of the TCR loci in T-cells, and the requirement for co-receptors (CD8 or CD4) in these interactions.

Using the model mouse T-cell antigen, chicken ovalbumin, and a cytolytic T-cell (CTL) receptor specific for this antigen (derived from the TCR-transgenic mouse model, OT-I) we have developed and validated a screening protocol and data analysis pipeline for large scale detection of CTL epitopes. The primary screening consists of co-incubating T-cells of interest and target cells. These target cells have been modified to carry short peptide coding sequences linked to a FRET reporter construct composed of CFP and YFP monomers separated by a granzyme-B-cleavable linker. When cognate peptides are recognized by T-cell receptors of interest, granzyme-B is transferred into the target cells carrying the immunogenic peptide. This

results in cleavage of the FRET reporter, which produces a shift in the optical properties of the cell, and allows us to select for these cells using fluorescence-activated cell sorting (FACS). Collected cells are then lysed and the lentiviral transgene is amplified for sequencing by next-generation methods to reveal the identity of peptide-coding sequences responsible for eliciting CTL-reactivity.

The specificity of the approach was validated by creating a positive-control cell line expressing the correct ovalbumin epitope (ID8.minOva) and a decoy cell line coding for a scrambled version of the epitope (ID8.minOScr). When mixed at a 1:1 ratio and subjected to OT-I CTL interrogation, nearly complete enrichment of the correct sequence was observed in the genomic DNA of collected cells **(Figure 8A)**. To assess the sensitivity of the method, a high-diversity library of completely random peptide-coding sequence was constructed. The positive control line (ID8.minOva) was spiked in to the random minigene encoding cell line at varying abundances and was similarly subjected to screening with OT-I CTL. With minimal optimization and only a single-round of screening (no additional panning rounds), Ova-coding sequences were detected above background at abundances as low as 100 ppm **(Figure 8B)**.

2.3 Current work: identifying the antigens recognized by TIL in HGSC

Based on the strong data generated by our DOD Teal Award, we were successful in obtaining new funding from Genome Canada, Genome British Columbia, and BC Cancer Foundation for our T cell antigen identification efforts **(see Leveraged Funding)**. Our next steps are to apply the above approach to detecting cognate antigens from tumor cDNA from the ovarian cancer subjects studied here as well as to characterize TCR cross-reactivity of tumor-reactive T-cells. We are starting by evaluating $CD8^+$ cytolytic T cells from patient ascites or bulk tumor. We will isolate $CD45^+$ from samples and expand these isolated lymphocytes *ex vivo*. From $CD45^-$ tumor cells, cDNA fragment libraries will be generated and used to create a library of cDNA-encoding lentivirus, which will be transduced into autologous B-cells (from patient blood samples). Transduced B-cells will then be subject to the screening and sequencing approach that has been validated above. Peptides encoded by positive hits will then be used to selectively enrich tumor-infiltrating or tumor-associated lymphocyte populations for use as increased-potency adoptive cell therapeutics. T-cell cross-reactivity is another important consideration that we will examine by using the above method to screen patient-derived T-cell clonal lines of interest against completely random peptide coding sequence. Though cross-reactivity is typically not observed in healthy individuals due to natural mechanisms of central and peripheral tolerance, mounting evidence has indicated that each T-cell receptor is capable of recognizing a vast array of unique sequences in complex with their complementary MHC molecule(s). Using random sequence that is not restricted to naturally occurring coding sequence, we will assess the level of cross-reactivity observed in highly tumor-reactive T-cells and work to develop a predictive metric that will provide insight into the probability of adverse events resulting from administration of highly cross-reactive T-cells versus relatively lower cross-reactive T-cells.

Task 3. To determine whether tumor-infiltrating B cells and T cells recognize the same antigens.

The goal of this task was to test the hypothesis that CD20+ TIL can serve as antigen presenting cells (APC) in the tumor microenvironment.

Progress:

As discussed in Task 1 (above), with this DOD Teal Award we learned that CD20+ TIL are highly polyclonal (compared to their plasma cell counterparts). This makes it far less likely that they serve as APC in the tumor microenvironment. Instead, we are exploring the potential

role of plasma cells in this process (as described in Task 1). As for CD20+ TIL, we are now investigating the alternative hypothesis that they serve as "organizers" of lymphocytic infiltrates by releasing immune stimulatory cytokines and chemokines in the tumor bed. With new, leveraged funding from the Canadian Institutes of Health Research (CIHR) **(see Leveraged Funding)**, we are using an innovative platform (Nanostring) to perform gene expression profiling of HGSC tumors that contain either (a) CD8+ TIL alone, or (b) CD8+ and CD20+ TIL together. From this work, we intend to identify immune stimulatory factors released by CD20+ TIL that enhance the anti-tumor effects of CD8+ TIL.

Task 4. To assess the functional phenotype of antigen-specific CD4+FoxP3+ TIL.

CD4+FoxP3+ TIL show great functional heterogeneity in EOC, which makes it difficult to draw definitive conclusions about their role in the tumor environment. With knowledge of their cognate antigens, we will be able to clarify this issue by assessing the functional phenotype of individual CD4+FoxP3+ T cell clones as opposed to bulk cell preparations. We proposed to do this by constructing MHC class II tetramers, which bind specifically to CD4+ T cells expressing TCRs relevant to a particular antigen.

Progress:

In flow cytometry experiments, we discovered that CD4+FoxP3+ TIL comprised two distinct populations that could be distinguished by their expression of CD25. In fact, the entire CD4+ TIL compartment could be subdivided into four subpopulations based on expression of FoxP3 and CD25 (**Figure 9)**. We performed additional flow cytometry experiments to assess the activation status and cytokine production profiles of these four CD4+ TIL subsets (n = 6 cases). CD25+FoxP3+ TIL had a classic regulatory T cell phenotype (**Figure 9)**. Unexpectedly, we discovered that the CD25+FoxP3- TIL subpopulation had a previously undescribed phenotype. On the one hand, they had an activated phenotype as evidenced by high CD69 and low CCR7 expression. In comparison to Tregs, CD25+FoxP3- TIL expressed similar levels of GITR; however, they expressed lower levels of CTLA-4 and OX40 and were negative for Helios (**Figure 9)**. These data suggested that CD25+FoxP3- cells might be Th1 cells, which are widely reported among TIL. However, CD25-+FoxP3- T cells failed to produce any of the hallmark Th1 cytokines IFN-γ, TNF-α or IL-2 after *in vitro* stimulation with PMA and ionomycin (**Figure 9C)**. Indeed, Th1 cytokines were only produced by the CD25-FoxP3- subset. None of the CD4+ TIL subsets produced IL-4 or IL-17A (not shown).

Given that CD25+FoxP3- T cells did not express canonical Th cytokines, we investigated the possibility that they might represent other less common CD4+ T cell phenotypes. CD4+ cytolytic T cells have been described in cancer; however, similar to other non-Treg cells, very few CD25+FoxP3- T cells expressed the cytolytic markers TIA-1, granzyme B or perforin (not shown). Furthermore, CD25+FoxP3- TIL did not express CXCR5, a marker of T follicular helper cells (not shown).

Based on their lack of discernible functional attributes, we hypothesized that CD25+FoxP3-TIL might be in a suppressed or exhausted state. In accord with this, we found that CD25+FoxP3- T cells expressed very high levels of the exhaustion marker PD-1 (**Figure 9D)**. Indeed, the level of PD-1 expressed by CD25+FoxP3- TIL was on average 3.1-fold higher than Tregs, and 6.6-fold higher than CD25-FoxP3- cells. In addition, CD25+FoxP3- TIL expressed the exhaustion markers LAG-3 (not shown) and TIM-3, the latter being found on cells with the highest PD-1 levels (**Figure 9D)**. Thus, CD25+FoxP3- TIL exhibited an exhausted phenotype based on the expression of these markers and deficient cytokine production.

To investigate the prognostic significance of TIL subsets, a 187-case HGSC TMA was stained with antibodies to CD8, CD25 and FoxP3 (**Figure 10**). Because CD4 is also expressed by macrophages, it is difficult to score CD4+ TIL directly. Instead, we assumed that any CD25+ and/or FoxP3+ cell that did not express CD8 was a CD4+ T cell, an assumption that was justified by flow cytometry (not shown). With this staining combination, we could directly visualize all CD8+ TIL subsets, as well as the CD25+FoxP3-, CD25+FoxP3+ and CD25-FoxP3+ subsets of CD4+ TIL. To infer the number of CD4+CD25-FoxP3- TIL, we employed a second IHC combination involving antibodies to CD3, CD8 and FoxP3. We determined the number of CD4+FoxP3- cells, which appeared as CD3+CD8-FoxP3- cells. From this, we subtracted the number of CD25+FoxP3- cells determined from the first staining combination. This yielded an estimate of the number of CD4+CD25-FoxP3- cells. Our detection and scoring approach proved valid, as the results obtained by multi-color IHC and flow cytometry were concordant. We stained an adjacent section of the TMA for cytokeratin to unequivocally identify tumor epithelium versus stroma; for all subsequent analyses we focused on intraepithelial TIL, as these have the greatest prognostic significance.

As expected, CD8+ TIL were strongly associated with disease-specific survival (HR = 0.33, P-value<0.0001; not shown) and progression free survival (HR = 0.38, P-value<0.0001) (**Figure 10A**). The strong prognostic effect of CD8+ TIL can confound the analysis of closely associated TIL subsets, such as Tregs. Therefore, to determine the prognostic significance of CD4+ TIL subsets, we restricted our analysis to cases that were positive for CD8+ TIL. As expected, cases with a higher than median ratio of Tregs to CD8+ TIL trended toward decreased survival (HR = 1.55, P-value=0.09) (**Figure 10B**). In contrast, a higher than median ratio of CD25+FoxP3- TIL to CD8+ TIL was strongly associated with survival (HR = 0.56, P-value=0.02) (**Figure 10C**). The prognostic effect of CD25+FoxP3- TIL was even more pronounced in cases with lower levels of Tregs (HR = 0.29, P-value=0.003) (**Figure 10D**). No other CD4+ TIL subsets showed an association with survival (not shown). Thus, the CD25+FoxP3- subset was unique among CD4+ TIL in showing a positive association with patient survival.

Thus, we have discovered a novel subset of CD4+ TIL that, like FoxP3+ TIL, express the activation marker CD25. Importantly, however, whereas CD25+FoxP3+ TIL are associated with poor prognosis (consistent with them being Tregs), CD25+FoxP3- T cells are associated with favorable prognosis. We now believe that these cells are responsible for the favorable prognosis that we previously attributed to FoxP3+ TIL. Thus, we intend to focus our antigen discovery efforts on this subset of CD4+ TIL using the novel high througput screen described in Task 3.

A manuscript describing the above findings was recently published in the AACR journal *Cancer Immunology Research.*

KEY RESEARCH ACCOMPLISHMENTS:

1) We published two manuscripts describing the results of the original IDEA award:

(a) Castellarin M, Milne K, Zeng T, Tse K, Mayo M, Zhao Y, Webb JR, Watson PH, Nelson BH, Holt RA. Clonal evolution of high-grade serous ovarian carcinoma from primary to recurrent disease. J Pathol. 2013 Mar;229(4):515-24. doi:10.1002/path.4105. Epub 2012 Nov 29. PubMed PMID: 22996961.

(b) Wick, D., Webb, J.R., Nielsen, J.S., Martin, S., Kroeger, D.R., Milne, K., Castellarin, M., Twumasi-Boateng, K., Watson, P.H., Holt, R.H., Nelson, B.H. 2014. Surveillance of

the tumor mutanome by T cells during progression from primary to recurrent ovarian cancer. *Clin Cancer Res.* Mar 1;20(5):1125-34. Epub 2013 Feb 7. PMID: 24323902.

2) We published a key manuscript describing our discovery of a prognostically favorable CD4+ T cell subset in ovarian cancer:

deLeeuw RJ, Kost SE, Kakal JA, **Nelson BH**. The prognostic value of FoxP3+ tumor-infiltrating lymphocytes in cancer: a critical review of the literature. Clin Cancer Res. 2012 Jun 1;18(11):3022-9. doi: 10.1158/1078-0432.CCR-11-3216. Epub 2012 Apr 17. Review. PubMed PMID: 22510350.

3) As listed below, from 2012-2015 our team published 25 manuscripts with direct relevance to this project, and 58 with indirect relevance.

4) Task 1: Illumina-based IgG profiling was completed for 3 patients at 3 time points.

5) Task 1: Robust methods were developed to amplify matched IgG heavy and light chains by single-cell RT-PCR, to clone CDR3 regions into IgG expression vectors, and to prepare recombinant IgG.

6) Task 1: We discovered that the bulk of IgG sequences from tumors are derived from plasma cells rather than CD20+ TIL. A manuscript describing these results is under review at *Clinical Cancer Research* **(Appendix A)**.

7) Task 1: Based on the above findings, our IgG cloning and antigen identification efforts are now directed toward these plasma cells instead of CD20+ B cells. We have obtained two new sources of peer-reviewed funding to continue this work **(see Leveraged Funding)**.

8) Task 2: Illumina-based profiling of TCRs was completed for 3 patients at 3 time points.

9) Task 2: Robust methods were developed to amplify paired TCR-alpha and –beta CDR3 regions by single-cell RT-PCR.

10) Task 2: Faced with an unexpectedly high diversity of TCR sequences among TIL, we elected to develop an entirely new high throughput method to identify the antigens recognized by TIL. This method will be applicable to not only this project, but many future projects by us and others. We have obtained new peer-reviewed funding to continue this work **(see Leveraged Funding)**.

11) Task 3: We discovered that CD20+ TIL are highly polyclonal, making it unlikely that they serve as antigen presenting cells. We have obtained new funding to investigate the alternative hypothesis that CD20+ TIL serve as “organizers” of lymphocytic infiltrates in tumor tissue, thereby enhancing CD8+ TIL responses **(see Leveraged Funding)**.

12) Task 4: This task was completed in 2013/2014, and a manuscript describing the results was published in *Cancer Immunology Research* **(see Reportable Outcomes).**

REPORTABLE OUTCOMES:

Manuscripts with direct relevance published by the team in 2012-2015 (n = 25; Teal Award PIs and co-PIs are shown in boldface):

1. Nielsen JS, Sahota RA, Milne K, Kost SE, Nesslinger NJ, **Watson PH**, **Nelson BH**. CD20+ tumor-infiltrating lymphocytes have an atypical CD27- memory phenotype and together with CD8+ T cells promote favorable prognosis in ovarian cancer. Clin Cancer Res. 2012 Jun 15;18(12):3281-92. doi: 10.1158/1078-0432.CCR-12-0234. Epub 2012 May 2. PubMed PMID: 22553348.

2. Nielsen JS, **Nelson BH**. Tumor-infiltrating B cells and T cells: Working together to promote patient survival. Oncoimmunology. 2012 Dec 1;1(9):1623-1625. PubMed PMID: 23264915; PubMed Central PMCID: PMC3525624.

3. Castellarin M, Milne K, Zeng T, Tse K, Mayo M, Zhao Y, **Webb JR**, **Watson PH**, **Nelson BH**, **Holt RA**. Clonal evolution of high-grade serous ovarian carcinoma from primary to recurrent disease. J Pathol. 2013 Mar;229(4):515-24. doi:10.1002/path.4105. Epub 2012 Nov 29. PubMed PMID: 22996961.

4. deLeeuw RJ, Kost SE, Kakal JA, **Nelson BH**. The prognostic value of FoxP3+ tumor-infiltrating lymphocytes in cancer: a critical review of the literature. Clin Cancer Res. 2012 Jun 1;18(11):3022-9. doi: 10.1158/1078-0432.CCR-11-3216. Epub 2012 Apr 17. Review. PubMed PMID: 22510350.

5. Warren RL, Choe G, Freeman DJ, Castellarin M, Munro S, Moore R, **Holt RA**. Derivation of HLA types from shotgun sequence datasets. Genome Med. 2012 Dec 10;4(12):95. [Epub ahead of print] PubMed PMID: 23228053; PubMed Central PMCID: PMC3580435.

6. Milne K, Alexander C, **Webb JR**, Sun W, Dillon K, Kalloger SE, Gilks CB, Clarke B, Köbel M, **Nelson BH**. Absolute lymphocyte count is associated with survival in ovarian cancer independent of tumor-infiltrating lymphocytes. J Transl Med. 2012 Feb 27;10:33. doi: 10.1186/1479-5876-10-33. PubMed PMID: 22369276; PubMed Central PMCID: PMC3310776.

7. **Nelson BH**. Killer T cells to the rescue in ovarian cancer. Gynecol Oncol. 2012 Feb;124(2):178-9. doi: 10.1016/j.ygyno.2011.12.434. PubMed PMID: 22264602.

8. Watson CT, Steinberg KM, Huddleston J, Warren RL, Malig M, Schein J, Willsey AJ, Joy JB, Scott JK, Graves TA, Wilson RK, **Holt RA**, Eichler EE, Breden F. Complete haplotype sequence of the human immunoglobulin heavy-chain variable, diversity, and joining genes and characterization of allelic and copy-number variation. Am J Hum Genet. 2013 Apr 4;92(4):530-46. doi: 10.1016/j.ajhg.2013.03.004. Epub 2013 Mar 28. PubMed PMID: 23541343; PubMed Central PMCID: PMC3617388.

9. West NR, Kost SE, Martin SD, Milne K, Deleeuw RJ, **Nelson BH, Watson PH**. Tumour-infiltrating FOXP3(+) lymphocytes are associated with cytotoxic immune responses and good clinical outcome in oestrogen receptor-negative breast cancer. Br J Cancer. 2013 Jan 15;108(1):155-62. doi: 10.1038/bjc.2012.524. Epub 2012 Nov 20. PubMed PMID: 23169287; PubMed Central PMCID: PMC3553524.

10. Woodsworth DJ, Castellarin M, **Holt RA**. Sequence analysis of T-cell repertoires in health and disease. Genome Med. 2013 Oct 30;5(10):98. doi: 10.1186/gm502. eCollection 2013. Review. PubMed PMID: 24172704; PubMed Central PMCID:PMC3979016.

11. Townsend KN, Spowart JE, Huwait H, Eshragh S, West NR, Elrick MA, Kalloger SE, Anglesio M, **Watson PH**, Huntsman DG, Lum JJ. Markers of T cell infiltration and function associate with favorable outcome in vascularized high-grade serous ovarian carcinoma. PLoS One. 2013 Dec 23;8(12):e82406. doi: 10.1371/journal.pone.0082406. eCollection 2013. PubMed PMID: 24376535; PubMed Central PMCID: PMC3871161.

12. Sharma G, **Holt RA**. T-cell epitope discovery technologies. Hum Immunol. 2014 Jun;75(6):514-9. doi: 10.1016/j.humimm.2014.03.003. Epub 2014 Apr 19. PubMed PMID: 24755351.

13. Brown SD, Warren RL, Gibb EA, Martin SD, Spinelli JJ, **Nelson BH, Holt RA**. Neo-antigens predicted by tumor genome meta-analysis correlate with increased patient survival. Genome

Res. 2014 May;24(5):743-50. doi: 10.1101/gr.165985.113. Epub 2014 Apr 29. PubMed PMID: 24782321; PubMed Central PMCID: PMC4009604.

14. Wick DA, **Webb JR**, Nielsen JS, Martin SD, Kroeger DR, Milne K, Castellarin M, Twumasi-Boateng K, **Watson PH, Holt RA, Nelson BH**. Surveillance of the tumor mutanome by T cells during progression from primary to recurrent ovarian cancer. Clin Cancer Res. 2014 Mar 1;20(5):1125-34. doi: 10.1158/1078-0432.CCR-13-2147. Epub 2013 Dec 9. PubMed PMID: 24323902.

15. **Webb JR**, Milne K, **Watson PH**, Deleeuw RJ, **Nelson BH**. Tumor-infiltrating lymphocytes expressing the tissue resident memory marker CD103 are associated with increased survival in high-grade serous ovarian cancer. Clin Cancer Res. 2014 Jan 15;20(2):434-44. doi: 10.1158/1078-0432.CCR-13-1877. Epub 2013 Nov 4. PubMed PMID: 24190978.

16. **Webb JR**, Milne K, **Nelson BH**. Location, location, location: CD103 demarcates intraepithelial, prognostically favorable CD8(+) tumor-infiltrating lymphocytes in ovarian cancer. Oncoimmunology. 2014 Jan 10;3:e27668. eCollection 2014. PubMed PMID: 25101220; PubMed Central PMCID: PMC4121334.

17. **Webb, JR**, Milne, K, **Nelson, BH**. PD-1 and CD103 are widely co-expressed on prognostically favourable intraepithelial CD8 T cells in human ovarian cancer. 2015. *Cancer Immunology Research.* Aug; 3(8):926-35. Epub 2015 May 8. PubMed PMID: 25957117.

18. Brown S, Raeburn L, **Holt RA**. Profiling tissue-resident T cell repertoires by RNA-seq. *Genome Medicine* 2015, 7:125 [Epub ahead of print]. PubMed PMID: 26620832.

19. **Holt RA**. Immunogenomics: a foundation for intelligent immune design. *Genome Medicine* 2015 Nov 19;7(1):116. PubMed PMID: 26582413.

20. **Nelson, B.H.** 2015. New insights into tumor immunity revealed by the unique genetic and genomic aspects of ovarian cancer. *Current Opinion in Immunology,* Apr; 33:93-100. PMID: 25710852.

21. Bowtell, DD, Boehm, S., Ahmed, A., Aspuria, P-J., Bas, R.C., Beral V., Berek, J.S., Birrer, M., Blagden, S., Bookman, M.A., Brenton, J., Chiappinelli, K.B., Martins, F.C., Coukos, G., Drapkin, R., Edmondson, R., Fotopoulou, C., Gabra, H., Galon, J., Gourley, C., Heong, V., Huntsman, D., Iwanicki, M., Karlan, B., Kaye, A., Lengyel, E., Levine, D.A., Lu, K., McNeish, I., Menon, U., Narod, S., **Nelson, BH,** Nephew, K., Pharoah, P., Powell, D., Ramos, P., Romero, I., Scott, C., Sood, A.K., Stronach, E.A., Balkwill, F. 2015. Rethinking ovarian cancer II: A roadmap for reducing mortality from high-grade serous ovarian cancer. *Nat Rev Cancer.* Oct 23;15(1):668-79. PMID:26493647.

22. Martin SD, Coukos G, **Holt RA**, **Nelson BH.** Targeting the undruggable: Immunotherapy meets personalized oncology in the genomic era. *Ann Oncol*. Dec; 26(12):2367-74. PMID: 26371284.

23. Nielsen, J.S., Martin, S.D., and **Nelson, BH** 2015. Personalized immunotherapy targeting the cancer mutanome. *Encyclopedia of Immunobiology (*Elsevier). Olja Finn (Section Editor) and Michael J. H. Ratcliffe (Editor in Chief). *In press.*

24. Webb, J.R., Milne, K., Kroeger, D.R., **Nelson, BH** 2015. PD-L1 expression is associated with tumor-infiltrating T cells and favorable prognosis in high-grade serous ovarian cancer. *Submitted.*

25. Kroeger, D.R., Milne, K., **Nelson, BH** 2015. Plasma cell infiltration identifies ovarian cancers with robust cytolytic T cell responses and superior prognosis. *Under review at Clinical Cancer Research.*

Manuscripts with indirect relevance published by the team in 2012-2015 (n = 58):

1. Sio A, Chehal MK, Tsai K, Fan X, Roberts ME, Nelson BH, Grembecka J, Cierpicki T, Krebs DL, Harder KW. Dysregulated hematopoiesis caused by mammary cancer is associated with epigenetic changes and hox gene expression in hematopoietic cells. Cancer Res. 2013 Oct 1;73(19):5892-904. doi:10.1158/0008-5472.CAN-13-0842. Epub 2013 Aug 1. PubMed PMID: 23913828.
2. West NR, Kost SE, Martin SD, Milne K, Deleeuw RJ, Nelson BH, Watson PH. Tumour-infiltrating FOXP3(+) lymphocytes are associated with cytotoxic immune responses and good clinical outcome in oestrogen receptor-negative breast cancer. Br J Cancer. 2013 Jan 15;108(1):155-62. doi: 10.1038/bjc.2012.524. Epub 2012 Nov 20. PubMed PMID: 23169287; PubMed Central PMCID: PMC3553524.
3. Cancer Genome Atlas Research Network. The Cancer Genome Atlas Pan-Cancer analysis project. Nat Genet. 2013 Sep 26;45(10):1113-20. doi: 10.1038/ng.2764. PubMed PMID: 24071849.
4. Yan Y, Li X, Blanchard A, Bramwell VH, Pritchard KI, Tu D, Shepherd L, Myal Y, Penner C, Watson PH, Leygue E, Murphy LC. Expression of both estrogen receptor-beta 1 (ER-β1) and its co-regulator steroid receptor RNA activator protein (SRAP) are predictive for benefit from tamoxifen therapy in patients with estrogen receptor-alpha (ER-α)-negative early breast cancer (EBC). Ann Oncol. 2013 Aug;24(8):1986-93. doi: 10.1093/annonc/mdt132. Epub 2013 Apr 11. PubMed PMID: 23579816.
5. Cancer Genome Atlas Research Network. Comprehensive molecular characterization of clear cell renal cell carcinoma. Nature. 2013 Jul 4;499(7456):43-9. doi: 10.1038/nature12222. Epub 2013 Jun 23. PubMed PMID: 23792563; PubMed Central PMCID: PMC3771322.
6. Cancer Genome Atlas Research Network. Genomic and epigenomic landscapes of adult de novo acute myeloid leukemia. N Engl J Med. 2013 May 30;368(22):2059-74. doi: 10.1056/NEJMoa1301689. Epub 2013 May 1. Erratum in: N Engl J Med. 2013 Jul 4;369(1):98. PubMed PMID: 23634996; PubMed Central PMCID: PMC3767041.
7. Cancer Genome Atlas Research Network. Integrated genomic characterization of endometrial carcinoma. Nature. 2013 May 2;497(7447):67-73. doi: 10.1038/nature12113. Erratum in: Nature. 2013 Aug 8;500(7461):242. PubMed PMID: 23636398; PubMed Central PMCID: PMC3704730.
8. West NR, Murray JI, Watson PH. Oncostatin-M promotes phenotypic changes associated with mesenchymal and stem cell-like differentiation in breast cancer. Oncogene. 2013 Apr 15. doi: 10.1038/onc.2013.105. [Epub ahead of print] PubMed PMID: 23584474.
9. Cancer Genome Atlas Network. Comprehensive molecular portraits of human breast tumours. Nature. 2012 Oct 4;490(7418):61-70. doi: 10.1038/nature11412. Epub 2012 Sep 23. PubMed PMID: 23000897; PubMed Central PMCID: PMC3465532.
10. Cancer Genome Atlas Research Network. Comprehensive genomic characterization of squamous cell lung cancers. Nature. 2012 Sep 27;489(7417):519-25. doi: 10.1038/nature11404. Epub 2012 Sep 9. Erratum in: Nature. 2012 Nov 8;491(7423):288. Rogers, Kristen [corrected to Rodgers, Kristen]. PubMed PMID: 22960745; PubMed Central PMCID: PMC3466113.

11. Spowart JE, Townsend KN, Huwait H, Eshragh S, West NR, Ries JN, Kalloger S, Anglesio M, Gorski SM, Watson PH, Gilks CB, Huntsman DG, Lum JJ. The Autophagy Protein LC3A Correlates with Hypoxia and is a Prognostic Marker of Patient Survival in Clear Cell Ovarian Cancer. J Pathol. 2012 Aug 27. doi: 10.1002/path.4090. [Epub ahead of print] PubMed PMID: 22926683.

12. Cancer Genome Atlas Network. Comprehensive molecular characterization of human colon and rectal cancer. Nature. 2012 Jul 18;487(7407):330-7. doi: 10.1038/nature11252. PubMed PMID: 22810696; PubMed Central PMCID: PMC3401966.

13. McAlpine JN, Porter H, Köbel M, Nelson BH, Prentice LM, Kalloger SE, Senz J, Milne K, Ding J, Shah SP, Huntsman DG, Gilks CB. BRCA1 and BRCA2 mutations correlate with TP53 abnormalities and presence of immune cell infiltrates in ovarian high-grade serous carcinoma. Mod Pathol. 2012 May;25(5):740-50. doi: 10.1038/modpathol.2011.211. Epub 2012 Jan 27. PubMed PMID: 22282309.

14. West NR, Murphy LC, Watson PH. Oncostatin M suppresses oestrogen receptor-α expression and is associated with poor outcome in human breast cancer. Endocr Relat Cancer. 2012 Apr 10;19(2):181-95. doi: 10.1530/ERC-11-0326. Print 2012 Apr. PubMed PMID: 22267707.

15. Castellarin M, Warren RL, Freeman JD, Dreolini L, Krzywinski M, Strauss J, Barnes R, Watson P, Allen-Vercoe E, Moore RA, Holt RA. Fusobacterium nucleatum infection is prevalent in human colorectal carcinoma. Genome Res. 2012 Feb;22(2):299-306. doi: 10.1101/gr.126516.111. Epub 2011 Oct 18. PubMed PMID: 22009989; PubMed Central PMCID: PMC3266037.

16. Madhurantakam C, Duru AD, Sandalova T, Webb JR, Achour A. Inflammation-associated nitrotyrosination affects TCR recognition through reduced stability and alteration of the molecular surface of the MHC complex. PLoS One. 2012;7(3):e32805. doi: 10.1371/journal.pone.0032805. Epub 2012 Mar 14. PubMed PMID: 22431983; PubMed Central PMCID: PMC3303804.

17. Sio A, Chehal MK, Tsai K, Fan X, Roberts ME, Nelson BH, Grembecka J, Cierpicki T, Krebs DL, Harder KW. Dysregulated hematopoiesis caused by mammary cancer is associated with epigenetic changes and hox gene expression in hematopoietic cells. Cancer Res. 2013 Oct 1;73(19):5892-904. doi: 10.1158/0008-5472.CAN-13-0842. Epub 2013 Aug 1. PubMed PMID: 23913828.

18. Cancer Genome Atlas Research Network, Weinstein JN, Collisson EA, Mills GB, Shaw KR, Ozenberger BA, Ellrott K, Shmulevich I, Sander C, Stuart JM. The Cancer Genome Atlas Pan-Cancer analysis project. Nat Genet. 2013 Oct;45(10):1113-20. doi: 10.1038/ng.2764. PubMed PMID: 24071849; PubMed Central PMCID: PMC3919969.

19. Yan Y, Li X, Blanchard A, Bramwell VH, Pritchard KI, Tu D, Shepherd L, Myal Y, Penner C, Watson PH, Leygue E, Murphy LC. Expression of both estrogen receptor-beta 1 (ER-β1) and its co-regulator steroid receptor RNA activator protein (SRAP) are predictive for benefit from tamoxifen therapy in patients with estrogen receptor-alpha (ER-α)-negative early breast cancer (EBC). Ann Oncol. 2013 Aug;24(8):1986-93. doi: 10.1093/annonc/mdt132. Epub 2013 Apr 11. PubMed PMID: 23579816.

20. Cheah S, O'Donoghue S, Daudt H, Dee S, LeBlanc J, Braun L, Barnes R, Vercauteren S, Boone RH, Watson PH. Permission to contact (PTC)--a strategy to enhance patient engagement in translational research. Biopreserv Biobank. 2013 Aug;11(4):245-52. doi: 10.1089/bio.2013.0023. PubMed PMID: 24845592.

21. Cancer Genome Atlas Research Network. Comprehensive molecular characterization of clear cell renal cell carcinoma. Nature. 2013 Jul 4;499(7456):43-9. doi: 0.1038/nature12222. Epub 2013 Jun 23. PubMed PMID: 23792563; PubMed Central PMCID: PMC3771322.

22. LeBlanc J, Dee S, Braun L, Daudt H, Cheah S, Watson PH. Impact of a Permission to Contact (PTC) platform on biobank enrollment and efficiency. Biopreserv Biobank. 2013 Jun;11(3):144-8. doi: 10.1089/bio.2013.0004. Epub 2013 May 31. PubMed PMID: 24850090.

23. Cancer Genome Atlas Research Network. Genomic and epigenomic landscapes of adult de novo acute myeloid leukemia. N Engl J Med. 2013 May 30;368(22):2059-74. doi: 10.1056/NEJMoa1301689. Epub 2013 May 1. Erratum in: N Engl J Med. 2013 Jul 4;369(1):98. PubMed PMID: 23634996; PubMed Central PMCID: PMC3767041.

24. Warren RL, Freeman DJ, Pleasance S, Watson P, Moore RA, Cochrane K, Allen-Vercoe E, Holt RA. Co-occurrence of anaerobic bacteria in colorectal carcinomas. Microbiome. 2013 May 15;1(1):16. doi: 10.1186/2049-2618-1-16. PubMed PMID: 24450771; PubMed Central PMCID: PMC3971631.

25. Cancer Genome Atlas Research Network, Kandoth C, Schultz N, Cherniack AD, Akbani R, Liu Y, Shen H, Robertson AG, Pashtan I, Shen R, Benz CC, Yau C, Laird PW, Ding L, Zhang W, Mills GB, Kucherlapati R, Mardis ER, Levine DA. Integrated genomic characterization of endometrial carcinoma. Nature. 2013 May 2;497(7447):67-73. doi: 10.1038/nature12113. Erratum in: Nature. 2013 Aug 8;500(7461):242. PubMed PMID: 23636398; PubMed Central PMCID: PMC3704730.

26. Watson CT, Steinberg KM, Huddleston J, Warren RL, Malig M, Schein J, Willsey AJ, Joy JB, Scott JK, Graves TA, Wilson RK, Holt RA, Eichler EE, Breden F. Complete haplotype sequence of the human immunoglobulin heavy-chain variable, diversity, and joining genes and characterization of allelic and copy-number variation. Am J Hum Genet. 2013 Apr 4;92(4):530-46. doi: 10.1016/j.ajhg.2013.03.004. Epub 2013 Mar 28. PubMed PMID: 23541343; PubMed Central PMCID: PMC3617388.

27. Le Page C, Köbel M, de Ladurantaye M, Rahimi K, Madore J, Babinszky S, Bachvarov DR, Bachvarova M, Beauchamp MC, Cass CE, Chadwick D, Colleen C, Damaraju S, Dufour J, Gotlieb WH, Kalloger SE, Portelance L, McAlpine JN, Matte I, Piché A, Shaw P, Roehrl MH, Vanderhyden BC, Watson PH, Huntsman DG, Provencher DM, Mes-Masson AM. Specimen quality evaluation in Canadian biobanks participating in the COEUR repository. Biopreserv Biobank. 2013 Apr;11(2):83-93. doi: 10.1089/bio.2012.0044. Erratum in: Biopreserv Biobank. 2013 Aug;11(4):257. Roehrl, Michael H A [added]. PubMed PMID: 24845429.

28. Branton WG, Ellestad KK, Maingat F, Wheatley BM, Rud E, Warren RL, Holt RA, Surette MG, Power C. Brain microbial populations in HIV/AIDS: α-proteobacteria predominate independent of host immune status. PLoS One. 2013;8(1):e54673. doi: 10.1371/journal.pone.0054673. Epub 2013 Jan 23. PubMed PMID: 23355888; PubMed Central PMCID: PMC3552853.

29. Watson CT, Steinberg KM, Graves TA, Warren RL, Malig M, Schein J, Wilson RK, Holt RA, Eichler EE, Breden F. Sequencing of the human IG light chain loci from a hydatidiform mole BAC library reveals locus-specific signatures of genetic diversity. Genes Immun. 2014 Oct 23. doi: 10.1038/gene.2014.56. [Epub ahead of print] PubMed PMID: 25338678.

30. Parfenov M, Pedamallu CS, Gehlenborg N, Freeman SS, Danilova L, Bristow CA, Lee S, Hadjipanayis AG, Ivanova EV, Wilkerson MD, Protopopov A, Yang L, Seth S, Song X, Tang J, Ren X, Zhang J, Pantazi A, Santoso N, Xu AW, Mahadeshwar H, Wheeler DA, Haddad

RI, Jung J, Ojesina AI, Issaeva N, Yarbrough WG, Hayes DN, Grandis JR, El-Naggar AK, Meyerson M, Park PJ, Chin L, Seidman JG, Hammerman PS, Kucherlapati R; the Cancer Genome Atlas Network; the Cancer Genome Atlas Network. Characterization of HPV and host genome interactions in primary head and neck cancers. Proc Natl Acad Sci U S A. 2014 Oct 13. pii: 201416074. [Epub ahead of print] PubMed PMID: 25313082.

31. Barnes RO, Schacter B, Kodeeswaran S, Watson PH. Funding sources for Canadian biorepositories: the role of user fees and strategies to help fill the gap. Biopreserv Biobank. 2014 Oct;12(5):300-5. doi: 10.1089/bio.2014.0052. Epub 2014 Oct 14. PubMed PMID: 25314324.

32. Cancer Genome Atlas Research Network. Comprehensive molecular characterization of gastric adenocarcinoma. Nature. 2014 Sep 11;513(7517):202-9. doi: 10.1038/nature13480. Epub 2014 Jul 23. PubMed PMID: 25079317; PubMed Central PMCID: PMC4170219.

33. Davis CF, Ricketts CJ, Wang M, Yang L, Cherniack AD, Shen H, Buhay C, Kang H, Kim SC, Fahey CC, Hacker KE, Bhanot G, Gordenin DA, Chu A, Gunaratne PH, Biehl M, Seth S, Kaipparettu BA, Bristow CA, Donehower LA, Wallen EM, Smith AB, Tickoo SK, Tamboli P, Reuter V, Schmidt LS, Hsieh JJ, Choueiri TK, Hakimi AA; Cancer Genome Atlas Research Network, Chin L, Meyerson M, Kucherlapati R, Park WY, Robertson AG, Laird PW, Henske EP, Kwiatkowski DJ, Park PJ, Morgan M, Shuch B, Muzny D, Wheeler DA, Linehan WM, Gibbs RA, Rathmell WK, Creighton CJ. The somatic genomic landscape of chromophobe renal cell carcinoma. Cancer Cell. 2014 Sep 8;26(3):319-30. doi: 10.1016/j.ccr.2014.07.014. Epub 2014 Aug 21. PubMed PMID: 25155756; PubMed Central PMCID: PMC4160352.

34. Matzke L, Dee S, Bartlett J, Damaraju S, Graham K, Johnston R, Mes-Masson AM, Murphy L, Shepherd L, Schacter B, Watson PH. A practical tool for modeling biospecimen user fees. Biopreserv Biobank. 2014 Aug;12(4):234-9. doi: 10.1089/bio.2014.0008. PubMed PMID: 25162459.

35. Cancer Genome Atlas Research Network. Comprehensive molecular profiling of lung adenocarcinoma. Nature. 2014 Jul 31;511(7511):543-50. doi: 10.1038/nature13385. Epub 2014 Jul 9. Erratum in: Nature. 2014 Oct 9;514(7521):262. Rogers, K [corrected to Rodgers, K]. PubMed PMID: 25079552.

36. Watson PH. Biobank classification: communicating biorepository diversity. Biopreserv Biobank. 2014 Jun;12(3):163-4. doi: 10.1089/bio.2014.1231. PubMed PMID: 24955732.

37. Braun L, Lesperance M, Mes-Massons AM, Tsao MS, Watson PH. Individual investigator profiles of biospecimen use in cancer research. Biopreserv Biobank. 2014 Jun;12(3):192-8. doi: 10.1089/bio.2013.0092. Epub 2014 Jun 11. PubMed PMID: 24918606.

38. McKinnon ML, Rozmus J, Fung SY, Hirschfeld AF, Del Bel KL, Thomas L, Marr N, Martin SD, Marwaha AK, Priatel JJ, Tan R, Senger C, Tsang A, Prendiville J, Junker AK, Seear M, Schultz KR, Sly LM, Holt RA, Patel MS, Friedman JM, Turvey SE. Combined immunodeficiency associated with homozygous MALT1 mutations. J Allergy Clin Immunol. 2014 May;133(5):1458-62, 1462.e1-7. doi: 10.1016/j.jaci.2013.10.045. Epub 2013 Dec 12. PubMed PMID: 24332264.

39. Cancer Genome Atlas Research Network. Comprehensive molecular characterization of urothelial bladder carcinoma. Nature. 2014 Mar 20;507(7492):315-22. doi: 10.1038/nature12965. Epub 2014 Jan 29. PubMed PMID: 24476821; PubMed Central PMCID: PMC3962515.

40. West NR, Murray JI, Watson PH. Oncostatin-M promotes phenotypic changes associated with mesenchymal and stem cell-like differentiation in breast cancer. Oncogene. 2014 Mar

20;33(12):1485-94. doi: 10.1038/onc.2013.105. Epub 2013 Apr 15. PubMed PMID: 23584474.

41. Watson PH, Nussbeck SY, Carter C, O'Donoghue S, Cheah S, Matzke LA, Barnes RO, Bartlett J, Carpenter J, Grizzle WE, Johnston RN, Mes-Masson AM, Murphy L, Sexton K, Shepherd L, Simeon-Dubach D, Zeps N, Schacter B. A framework for biobank sustainability. Biopreserv Biobank. 2014 Feb;12(1):60-8. doi: 10.1089/bio.2013.0064. PubMed PMID: 24620771; PubMed Central PMCID: PMC4150367.

42. de Leeuw CN, Dyka FM, Boye SL, Laprise S, Zhou M, Chou AY, Borretta L, McInerny SC, Banks KG, Portales-Casamar E, Swanson MI, D'Souza CA, Boye SE, Jones SJ, Holt RA, Goldowitz D, Hauswirth WW, Wasserman WW, Simpson EM. Targeted CNS Delivery Using Human MiniPromoters and Demonstrated Compatibility with Adeno-Associated Viral Vectors. Mol Ther Methods Clin Dev. 2014 Jan 8;1:5. PubMed PMID: 24761428; PubMed Central PMCID: PMC3992516.

43. Johnson LD, Nesslinger NJ, Blood PA, Chima N, Richier LR, Ludgate C, Pai HH, Lim JT, Nelson BH, Vlachaki MT, Lum JJ. Tumor-associated autoantibodies correlate with poor outcome in prostate cancer patients treated with androgen deprivation and external beam radiation therapy. Oncoimmunology. 2014 Jun 25;3:e29243. eCollection 2014. PubMed PMID: 25114831; PubMed Central PMCID: PMC4125379.

44. Schmouth JF, Castellarin M, Laprise S, Banks KG, Bonaguro RJ, McInerny SC, Borretta L, Amirabbasi M, Korecki AJ, Portales-Casamar E, Wilson G, Dreolini L, Jones SJ, Wasserman WW, Goldowitz D, Holt RA, Simpson EM. Non-coding-regulatory regions of human brain genes delineated by bacterial artificial chromosome knock-in mice. BMC Biol. 2013 Oct 14;11:106. doi: 10.1186/1741-7007-11-106. PubMed PMID: 24124870; PubMed Central PMCID: PMC4015596.

45. Nielsen JS, Sedgwick C, Shahid A, Zong Z, Brumme ZL, Yu S, Liu L, Kroeger DR, Treon SP, Connors JM, Gascoyne RD, Berry BR, Marra MA, Morin RD, Macpherson N, Nelson BH. Toward personalized lymphoma immunotherapy: Identification of common driver mutations recognized by patient CD8+ T cells. Clin Cancer Res. 2015 Dec 2. pii: clincanres.2023.2015. [Epub ahead of print] PubMed PMID: 26631611.

46. Cancer Genome Atlas Research Network. The Molecular Taxonomy of Primary Prostate Cancer. Cell. 2015 Nov 5;163(4):1011-25. doi: 10.1016/j.cell.2015.10.025. PubMed PMID: 26544944.

47. Linehan WM, Spellman PT, Ricketts CJ, Creighton CJ, Fei SS, Davis C, Wheeler DA, Murray BA, Schmidt L, Vocke CD, Peto M, Al Mamun AA, Shinbrot E, Sethi A, Brooks S, Rathmell WK, Brooks AN, Hoadley KA, Robertson AG, Brooks D, Bowlby R, Sadeghi S, Shen H, Weisenberger DJ, Bootwalla M, Baylin SB, Laird PW, Cherniack AD, Saksena G, Haake S, Li J, Liang H, Lu Y, Mills GB, Akbani R, Leiserson MD, Raphael BJ, Anur P, Bottaro D, Albiges L, Barnabas N, Choueiri TK, Czerniak B, Godwin AK, Hakimi AA, Ho TH, Hsieh J, Ittmann M, Kim WY, Krishnan B, Merino MJ, Shaw KR, Reuter VE, Reznik E, Shelley CS, Shuch B, Signoretti S, Srinivasan R, Tamboli P, Thomas G, Tickoo S, Burnett K, Crain D, Gardner J, Lau K, Mallery D, Morris S, Paulauskis JD, Penny RJ, Shelton C, Shelton WT, Sherman M, Thompson E, Yena P, Avedon MT, Bowen J, Gastier-Foster JM, Gerken M, Leraas KM, Lichtenberg TM, Ramirez NC, Santos T, Wise L, Zmuda E, Demchok JA, Felau I, Hutter CM, Sheth M, Sofia HJ, Tarnuzzer R, Wang Z, Yang L, Zenklusen JC, Zhang J, Ayala B, Baboud J, Chudamani S, Liu J, Lolla L, Naresh R, Pihl T, Sun Q, Wan Y, Wu Y, Ally A, Balasundaram M, Balu S, Beroukhim R, Bodenheimer T, Buhay C, Butterfield YS, Carlsen R, Carter SL, Chao H, Chuah E, Clarke A, Covington KR, Dahdouli M, Dewal N,

Dhalla N, Doddapaneni HV, Drummond JA, Gabriel SB, Gibbs RA, Guin R, Hale W, Hawes A, Hayes DN, Holt RA, Hoyle AP, Jefferys SR, Jones SJ, Jones CD, Kalra D, Kovar C, Lewis L, Li J, Ma Y, Marra MA, Mayo M, Meng S, Meyerson M, Mieczkowski PA, Moore RA, Morton D, Mose LE, Mungall AJ, Muzny D, Parker JS, Perou CM, Roach J, Schein JE, Schumacher SE, Shi Y, Simons JV, Sipahimalani P, Skelly T, Soloway MG, Sougnez C, Tam A, Tan D, Thiessen N, Veluvolu U, Wang M, Wilkerson MD, Wong T, Wu J, Xi L, Zhou J, Bedford J, Chen F, Fu Y, Gerstein M, Haussler D, Kasaian K, Lai P, Ling S, Radenbaugh A, Van Den Berg D, Weinstein JN, Zhu J, Albert M, Alexopoulou I, Andersen JJ, Auman JT, Bartlett J, Bastacky S, Bergsten J, Blute ML, Boice L, Bollag RJ, Boyd J, Castle E, Chen YB, Cheville JC, Curley E, Davies B, DeVolk A, Dhir R, Dike L, Eckman J, Engel J, Harr J, Hrebinko R, Huang M, Huelsenbeck-Dill L, Iacocca M, Jacobs B, Lobis M, Maranchie JK, McMeekin S, Myers J, Nelson J, Parfitt J, Parwani A, Petrelli N, Rabeno B, Roy S, Salner AL, Slaton J, Stanton M, Thompson RH, Thorne L, Tucker K, Weinberger PM, Winemiller C, Zach LA, Zuna R; Cancer Genome Atlas Research Network. Comprehensive Molecular Characterization of Papillary Renal-Cell Carcinoma. N Engl J Med. 2015 Nov 4. [Epub ahead of print] PubMed PMID: 26536169.

48. Ciriello G, Gatza ML, Beck AH, Wilkerson MD, Rhie SK, Pastore A, Zhang H, McLellan M, Yau C, Kandoth C, Bowlby R, Shen H, Hayat S, Fieldhouse R, Lester SC, Tse GM, Factor RE, Collins LC, Allison KH, Chen YY, Jensen K, Johnson NB, Oesterreich S, Mills GB, Cherniack AD, Robertson G, Benz C, Sander C, Laird PW, Hoadley KA, King TA; TCGA Research Network, Perou CM. Comprehensive Molecular Portraits of Invasive Lobular Breast Cancer. Cell. 2015 Oct 8;163(2):506-19. doi: 10.1016/j.cell.2015.09.033. PubMed PMID: 26451490; PubMed Central PMCID: PMC4603750.

49. Meredith AJ, Slotty A, Matzke L, Babinszky S, Watson PH. A Model to Estimate Frozen Tissue Collection Targets in Biobanks to Support Cancer Research. Biopreserv Biobank. 2015 Oct;13(5):356-62. doi: 10.1089/bio.2014.0081. Epub 2015 Sep 29. PubMed PMID: 26418967.

50. Nelson BH, McAlpine JN. The more tumors change, the more they stay tame: do T cells keep POLE ultramutated endometrial carcinomas in check? Gynecol Oncol. 2015 Jul;138(1):1-2. doi: 10.1016/j.ygyno.2015.06.004. PubMed PMID: 26072691.

51. Cancer Genome Atlas Research Network, Brat DJ, Verhaak RG, Aldape KD, Yung WK, Salama SR, Cooper LA, Rheinbay E, Miller CR, Vitucci M, Morozova O, Robertson AG, Noushmehr H, Laird PW, Cherniack AD, Akbani R, Huse JT, Ciriello G, Poisson LM, Barnholtz-Sloan JS, Berger MS, Brennan C, Colen RR, Colman H, Flanders AE, Giannini C, Grifford M, Iavarone A, Jain R, Joseph I, Kim J, Kasaian K, Mikkelsen T, Murray BA, O'Neill BP, Pachter L, Parsons DW, Sougnez C, Sulman EP, Vandenberg SR, Van Meir EG, von Deimling A, Zhang H, Crain D, Lau K, Mallery D, Morris S, Paulauskis J, Penny R, Shelton T, Sherman M, Yena P, Black A, Bowen J, Dicostanzo K, Gastier-Foster J, Leraas KM, Lichtenberg TM, Pierson CR, Ramirez NC, Taylor C, Weaver S, Wise L, Zmuda E, Davidsen T, Demchok JA, Eley G, Ferguson ML, Hutter CM, Mills Shaw KR, Ozenberger BA, Sheth M, Sofia HJ, Tarnuzzer R, Wang Z, Yang L, Zenklusen JC, Ayala B, Baboud J, Chudamani S, Jensen MA, Liu J, Pihl T, Raman R, Wan Y, Wu Y, Ally A, Auman JT, Balasundaram M, Balu S, Baylin SB, Beroukhim R, Bootwalla MS, Bowlby R, Bristow CA, Brooks D, Butterfield Y, Carlsen R, Carter S, Chin L, Chu A, Chuah E, Cibulskis K, Clarke A, Coetzee SG, Dhalla N, Fennell T, Fisher S, Gabriel S, Getz G, Gibbs R, Guin R, Hadjipanayis A, Hayes DN, Hinoue T, Hoadley K, Holt RA, Hoyle AP, Jefferys SR, Jones S, Jones CD, Kucherlapati R, Lai PH, Lander E, Lee S, Lichtenstein L, Ma Y, Maglinte DT, Mahadeshwar HS, Marra MA, Mayo M, Meng S, Meyerson ML, Mieczkowski PA, Moore RA, Mose LE, Mungall AJ, Pantazi A, Parfenov M, Park PJ, Parker JS, Perou CM, Protopopov A, Ren X, Roach J, Sabedot TS,

Schein J, Schumacher SE, Seidman JG, Seth S, Shen H, Simons JV, Sipahimalani P, Soloway MG, Song X, Sun H, Tabak B, Tam A, Tan D, Tang J, Thiessen N, Triche T Jr, Van Den Berg DJ, Veluvolu U, Waring S, Weisenberger DJ, Wilkerson MD, Wong T, Wu J, Xi L, Xu AW, Yang L, Zack TI, Zhang J, Aksoy BA, Arachchi H, Benz C, Bernard B, Carlin D, Cho J, DiCara D, Frazer S, Fuller GN, Gao J, Gehlenborg N, Haussler D, Heiman DI, Iype L, Jacobsen A, Ju Z, Katzman S, Kim H, Knijnenburg T, Kreisberg RB, Lawrence MS, Lee W, Leinonen K, Lin P, Ling S, Liu W, Liu Y, Liu Y, Lu Y, Mills G, Ng S, Noble MS, Paull E, Rao A, Reynolds S, Saksena G, Sanborn Z, Sander C, Schultz N, Senbabaoglu Y, Shen R, Shmulevich I, Sinha R, Stuart J, Sumer SO, Sun Y, Tasman N, Taylor BS, Voet D, Weinhold N, Weinstein JN, Yang D, Yoshihara K, Zheng S, Zhang W, Zou L, Abel T, Sadeghi S, Cohen ML, Eschbacher J, Hattab EM, Raghunathan A, Schniederjan MJ, Aziz D, Barnett G, Barrett W, Bigner DD, Boice L, Brewer C, Calatozzolo C, Campos B, Carlotti CG Jr, Chan TA, Cuppini L, Curley E, Cuzzubbo S, Devine K, DiMeco F, Duell R, Elder JB, Fehrenbach A, Finocchiaro G, Friedman W, Fulop J, Gardner J, Hermes B, Herold-Mende C, Jungk C, Kendler A, Lehman NL, Lipp E, Liu O, Mandt R, McGraw M, Mclendon R, McPherson C, Neder L, Nguyen P, Noss A, Nunziata R, Ostrom QT, Palmer C, Perin A, Pollo B, Potapov A, Potapova O, Rathmell WK, Rotin D, Scarpace L, Schilero C, Senecal K, Shimmel K, Shurkhay V, Sifri S, Singh R, Sloan AE, Smolenski K, Staugaitis SM, Steele R, Thorne L, Tirapelli DP, Unterberg A, Vallurupalli M, Wang Y, Warnick R, Williams F, Wolinsky Y, Bell S, Rosenberg M, Stewart C, Huang F, Grimsby JL, Radenbaugh AJ, Zhang J. Comprehensive Integrative Genomic Analysis of Diffuse Lower-Grade Gliomas. N Engl J Med. 2015 Jun 25;372(26):2481-98. doi: 10.1056/NEJMoa1402121. Epub 2015 Jun 10. PubMed PMID: 26061751; PubMed Central PMCID: PMC4530011.

52. Cancer Genome Atlas Network. Genomic Classification of Cutaneous Melanoma. Cell. 2015 Jun 18;161(7):1681-96. doi: 10.1016/j.cell.2015.05.044. PubMed PMID: 26091043; PubMed Central PMCID: PMC4580370.

53. Castillo-Pelayo T, Babinszky S, LeBlanc J, Watson PH. The importance of biobanking in cancer research. Biopreserv Biobank. 2015 Jun;13(3):172-7. doi: 10.1089/bio.2014.0061. PubMed PMID: 26035006.

54. Twa DD, Mottok A, Chan FC, Ben-Neriah S, Woolcock BW, Tan KL, Mungall AJ, McDonald H, Zhao Y, Lim RS, Nelson BH, Milne K, Shah SP, Morin RD, Marra MA, Scott DW, Gascoyne RD, Steidl C. Recurrent genomic rearrangements in primary testicular lymphoma. J Pathol. 2015 Jun;236(2):136-41. doi: 10.1002/path.4522. Epub 2015 Mar 26. PubMed PMID: 25712539.

55. Murray JI, West NR, Murphy LC, Watson PH. Intratumoural inflammation and endocrine resistance in breast cancer. Endocr Relat Cancer. 2015 Feb;22(1):R51-67. doi: 10.1530/ERC-14-0096. Epub 2014 Nov 17. Review. PubMed PMID: 25404688.

56. Cancer Genome Atlas Network. Comprehensive genomic characterization of head and neck squamous cell carcinomas. Nature. 2015 Jan 29;517(7536):576-82. doi: 10.1038/nature14129. PubMed PMID: 25631445; PubMed Central PMCID: PMC4311405.

57. Watson CT, Steinberg KM, Graves TA, Warren RL, Malig M, Schein J, Wilson RK, Holt RA, Eichler EE, Breden F. Sequencing of the human IG light chain loci from a hydatidiform mole BAC library reveals locus-specific signatures of genetic diversity. Genes Immun. 2015 Jan-Feb;16(1):24-34. doi: 10.1038/gene.2014.56. Epub 2014 Oct 23. PubMed PMID: 25338678; PubMed Central PMCID: PMC4304971.

58. Gibb EA, Warren RL, Wilson GW, Brown SD, Robertson GA, Morin GB, Holt RA. Activation of an endogenous retrovirus-associated long non-coding RNA in human adenocarcinoma.

Genome Med. 2015 Mar 5;7(1):22. doi: 10.1186/s13073-015-0142-6. eCollection 2015. PubMed PMID: 25821520; PubMed Central PMCID: PMC4375928.

Leveraged Funding:

From 2012/2015, we obtained six new grants that are directly relevant to ovarian cancer immunology/immunotherapy:

1. How does the immune system contend with intratumoral heterogeneity?
Source: Canadian Cancer Society Research Institute
Dates: 02/2014 – 01/2016 Term: 2 years
PI: **Brad Nelson**
Co-PIs: **Rob Holt** and Sohrab Shah
The major goal of this project is to understand how the immune system controls tumor progression despite the presence of multiple tumor lineages within ovarian cancer patients.

2. What proportion of mutations in the ovarian cancer genome can be recognized by the immune system?
Source: Cancer Research Society
Dates: 10/2014 – 09/2016 Term: 2 years
PI: **Brad Nelson**
The major goal of this project is to determine whether ovarian tumors express mutated antigens that can potentially be recognized by CD8+ T cells and targeted by immunotherapy.

3. Mechanisms of protective immunity in ovarian cancer
Source: Canadian Institutes of Health Research (CIHR)
Dates: 10/2014 – 03/2015 Term: 1 year (bridge funding)
PI: **Brad Nelson**
Co-PI: **Rob Holt**
The major goal of this project is to define the mechanisms by which tumor-infiltrating T cells and B cells work together to promote effective tumor immunity in the setting of high-grade serous ovarian cancer.

4. Mechanisms of protective immunity in Ovarian Cancer
Source: Canadian Institutes of Health Research
Dates: May 2015 – Jun 2020 Term: 5 years (full award)
PI: **Brad Nelson**
Co-PI: **Rob Holt**
The major goal of this project is to define the mechanisms by which tumor-infiltrating T cells and B cells work together to promote effective tumor immunity in the setting of high-grade serous ovarian cancer.

5. A phase I study evaluating the feasibility and safety of infusion of autologous Tumour-Infiltrating Lymphocytes (TILs) with low-dose interleukin-2 therapy in patients with recurrent, persistent locally advanced metastatic cervical carcinoma or platinum-resistant ovarian cancer
Source: BC Cancer Foundation
Dates: Mar 2015 – Feb 2018 Term: 3 years
Co-PIs: **Brad Nelson, Rob Holt** and Anna Tinker
Co-applicants: John Webb, Raewyn Broday
The major goal of this project is to conduct a Phase I clinical trial of adoptive T cell therapy for platinum resistant HGSC (and metastatic cervical cancer).

6. The Immunotherapy network (iTNT): Targeting Ovarian Cancer (pending)
Source: Terry Fox Research Institute
Dates: Mar 2016 – Feb 2021 Term: 5 years
PI: **Pamela Ohashi**
Co-PI: **Brad Nelson**
Co-applicants: **Rob Holt** (and 12 others)
The major goal of this project is to develop more effective immunotherapies for HGSC by defining the major immune suppressive mechanisms and target antigens relevant to this disease.
*Note that this proposal is still under review. However, we are the only applicants for this funding mechanism, which was by invitation only. Therefore, there is virtually a 100% chance of success.

We also obtained 7 grants with indirect relevance to this project:

1. Targeting the Breast Cancer Genome with Personalized Therapeutic Vaccines
Source: Canadian Breast Cancer Foundation BC/Yukon
Dates: 08/2012 – 07/2015 Term: 3 years
PI: **Brad Nelson**
Co-PI: **Rob Holt**
The major goal of this project is to use genome and transcriptome sequencing data to design personalized cancer vaccines that target mutations and destroy spontaneous mammary tumours.

2. The mutated lymphoma genome: a target for therapeutic vaccination
Source: Canadian Cancer Society Research Institute
Dates: 02/2013 – 01/2015 Term: 2 years
PI: **Brad Nelson**
The major goal of this project is to assess the immunogenicity of the lymphoma genome and develop personalized therapeutic vaccines.

3. Small-molecule inhibitors of the PD1-PDL1 interaction for treating metastatic cancer
Source: Canadian Cancer Society Research Institute
Dates: 02/2013 – 01/2015 Term: 2 years
PI: Jeremy Wulff,
Co-applicant: **Brad Nelson**
The major goal of this project is to develop small molecules that enhance anti-tumor T cell responses by inhibiting the PD1-PDL1 interaction.

4. Mutant MYD88: A target for adoptive T cell therapy of WM
Source: The Waldenstrom's Macroglobulinemia Foundation of Canada and the International Waldenstrom's Macroglobulinemia Foundation (IWMF)
Dates: 10/2014 – 09/2016 Term: 2 years
PI: **Brad Nelson**
The major goal of this project is to develop and validate TCR contructs that will allow us to engineer CD8+ T cells to specifically recognize a common mutation in Waldenstrom's Macroglobulinemia (MYD88L265P).

5. Mutation Reactive Autologous T cells for the Treatment of Pancreatic Cancer
Source: Pancreas Centre BC, BC Cancer Foundation

Dates: Sept 1, 2014 – January 31, 2017 Term: 2.5 years
PI: **Rob Holt**
The main goal of this project is to develop an immune-based pancreatic ductal adenocarcinoma treatment that will reduce the chance of cancer recurrence in these patients.

6. Arming lymphocytes to kill apoptosis resistant cancer cells
Source: Canadian Cancer Society Research Institute
Dates: February 1, 2015 – January 31, 2018 Term: 3 years
PI: **Rob Holt**
Co-PIs: **Brad Nelson**, Jonathan Choy
The goal of this project is to engineer the granzyme-perforin pathway of cytotoxic lymphocytes to deliver to recipient tumor cells an alternative cytotoxic protein that can kill by apoptosis-independent mechanisms.

7. Methods and Technology Development at the Sequencing Platform at the BC Cancer Agency Genome Sciences Centre
Source: Genome Canada, Genome British Columbia, BC Cancer Foundation
Dates: October 1, 2015 – September 30, 2017 Term: 2 years
PI: **Rob Holt**
Co-PIs: Marco Marra, Steven Jones, Inanc Birol, Carl Hansen, Ryan Morin and others
One of the goals of this project is to expand the immunogenomics capabilities of the Genome Canada sequencing platform at the Genome Sciences Centre by incorporating next-generation sequencing (NGS) based HLA typing and the new methods for NGS based T-cell epitope discovery, developed as part of the current project.

CONCLUSION:

Overall, this study was a highly successful study. We discovered two new subsets of prognostically important lymphocytes in HGSC (plasma cells and CD25+FoxP3- CD4+ T cells). We developed novel, efficient methods to analyze T cell and B cell repertoires, isolate tumor-derived antibodies, and identify T cell antigens. We published 25 peer-reviewed manuscripts with direct relevance to this project and 58 with indirect relevance. We competed successfully for additional funding to carry this work forward and expand to other tumor sites (6 directly relevant grants, and 7 indirectly relevant grants). Based on the results of our Idea and Teal Awards, we are developing a Phase I clinical trial of adoptive T cell therapy for platinum-resistant HGSC. We have secured over $4M in funding for this trial and the required infrastructure from the BC Cancer Foundation. We expect to treat our first HGSC patient in early 2017. We are very grateful to the CDMRP for generously providing both the Idea and Teal Awards to enhance the strength of our Cancer Immunotherapy Program.

APPENDICES:

A. Kroeger, D.R., Milne, K., **Nelson, BH** 2015. Plasma cell infiltration identifies ovarian cancers with robust cytolytic T cell responses and superior prognosis. *Under review at Clinical Cancer Research.*

REFERENCES:

N/A

SUPPORTING DATA:

None.

FIGURES:

See following pages.

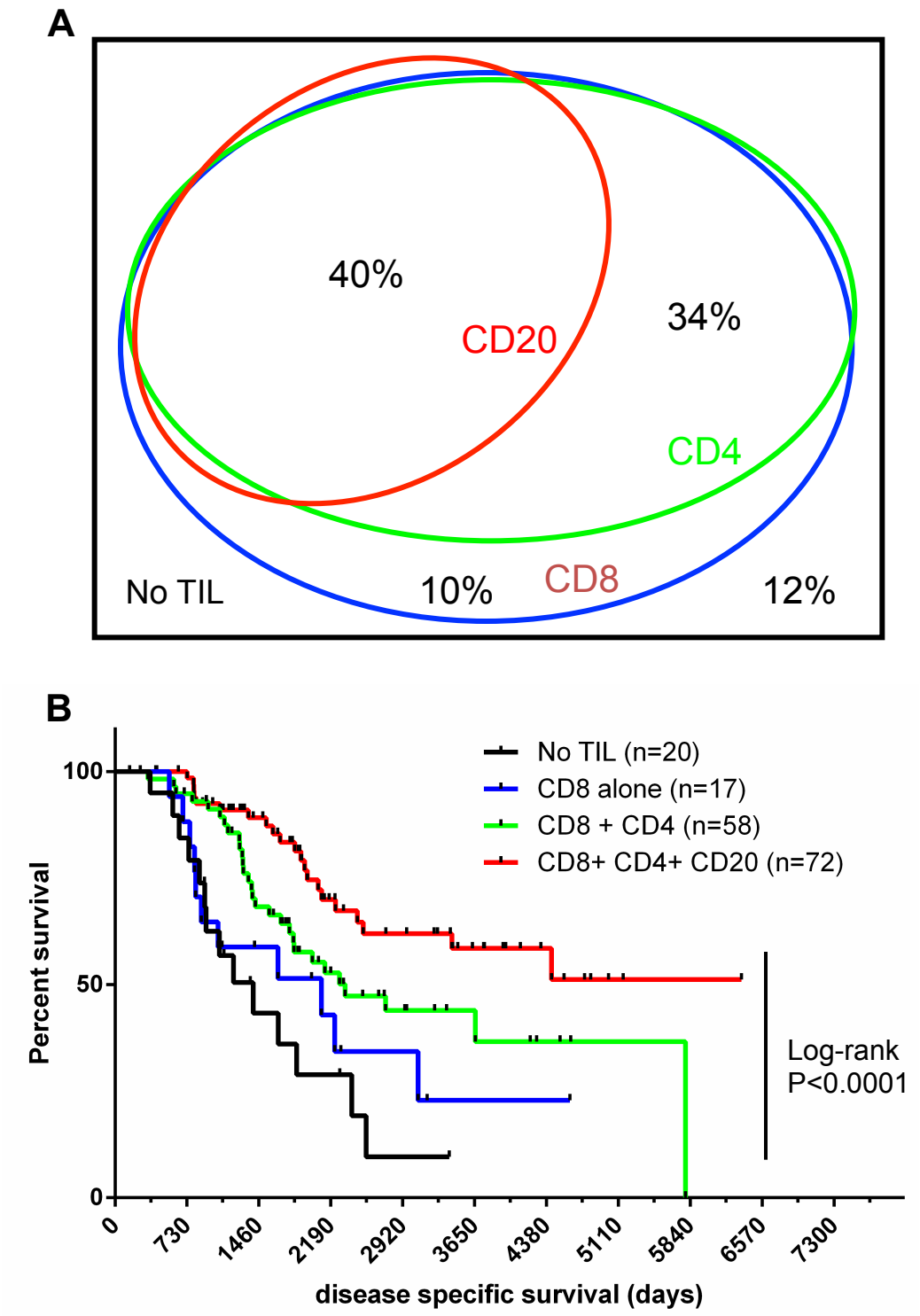

Figure 1. The distribution of TIL in HGSC and their association with long-term survival. **A)** Venn diagram showing the proportional distribution of CD8+, CD4+, and CD20+ TIL in 172 cases of optimally de-bulked HGSC as detected by IHC of a tumor tissue microarray as per Milne et al. 2009. **B)** Kaplan-Meier analysis of overall survival of patients shown in panel A. A small number of cases (n=5) do not fit into the four categories described.

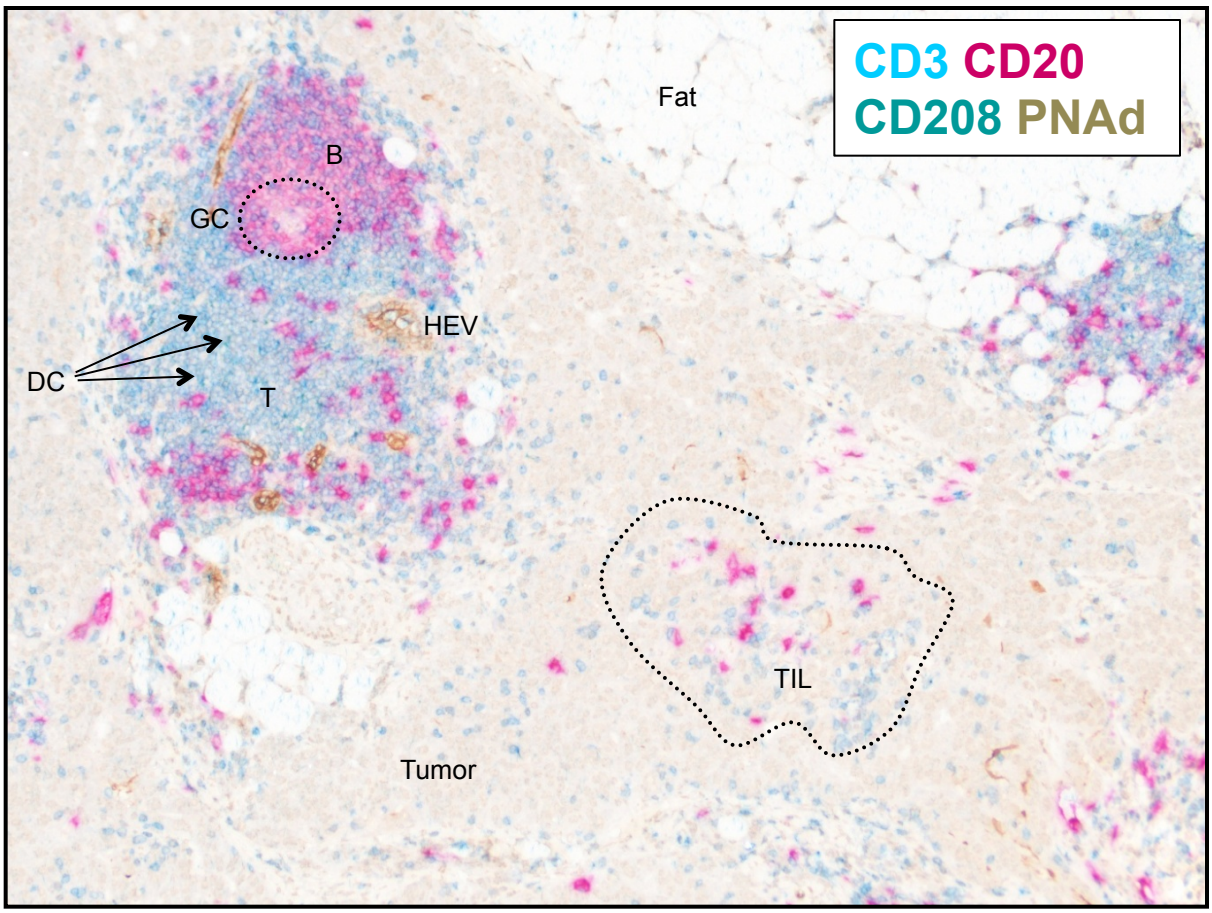

Figure 2. Tertiary lymphoid structure (TLS) and surrounding TIL in HGSC. Four-colour IHC image of a tumor section. CD20+ B cells appear red and a B cell follicle, marked "B", is found within the TLS structure. CD3+ T cells appear blue and the T cell zone of the TLS is marked "T". Both B cells and T cells are also found within the tumor epithelial region, examples of which are marked "TIL". High endothelial venules, marked "HEV", appear brown and were detected with an antibody to peripheral node addressin; these are located within the T cell zone of the TLS. Activated conventional dendritic cells, "DC", were detected with an antibody to CD208 and appear green-blue; they are located primarily within the T cell zone of the TLS (examples are indicated with arrows). A germinal center, "GC", is found within the B cell follicle. As expected, CD20 staining intensity is decreased within the GC due to physiological down-regulation of the CD20 protein on activated GC B cells.

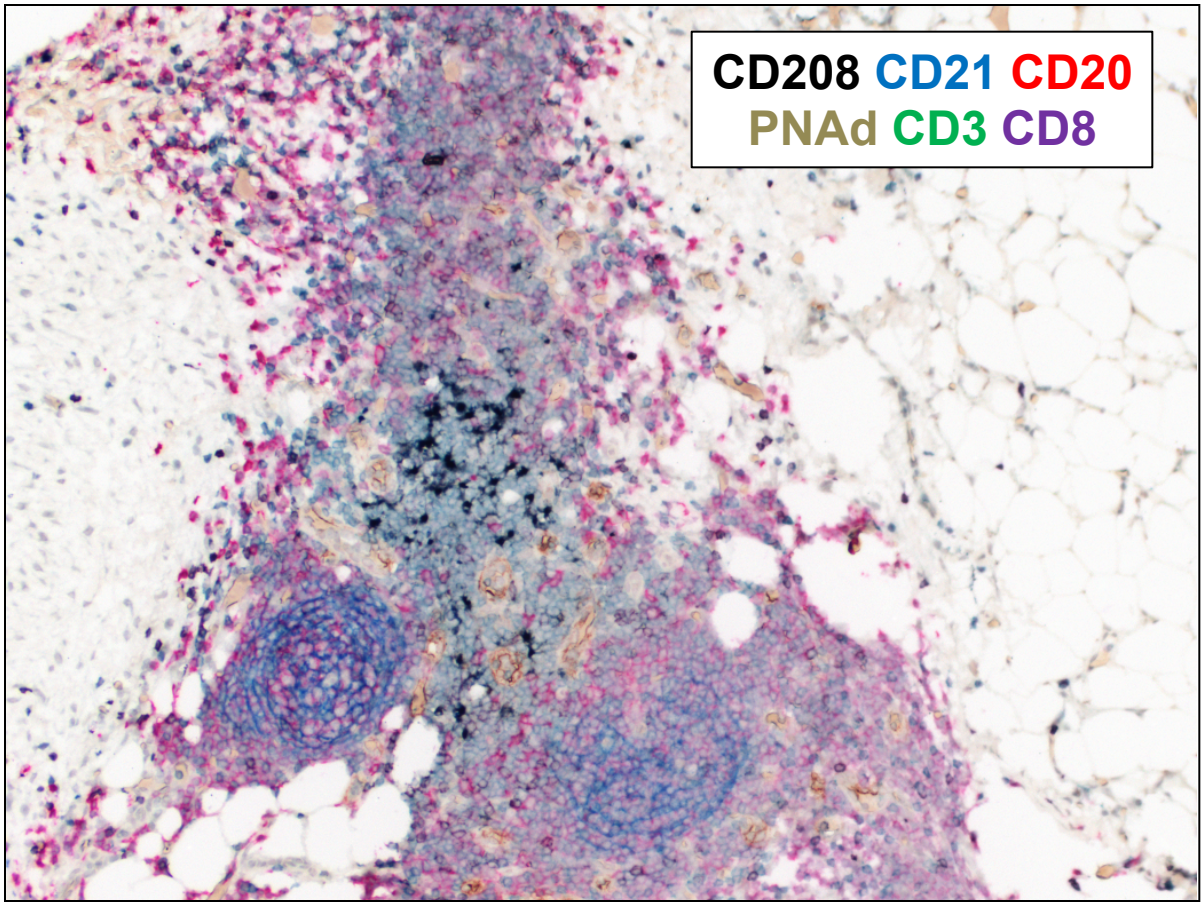

Figure 3. **Tertiary lymphoid structures contain germinal centres.** Six color immuno-histochemistry using antibodies to the indicated markers was used to investigate the cellular components of tertiary lymphoid structures. We observed that most well-defined B cell follicle structures contained interdigitating networks of CD21+ follicular DCs (blue), indicating they are germinal centers. Additional staining, not shown here, demonstrated the presence of activation-induced cytidine deaminase (AID) positive B cells and BCL-6+ T follicular helper cells within these germinal centers.

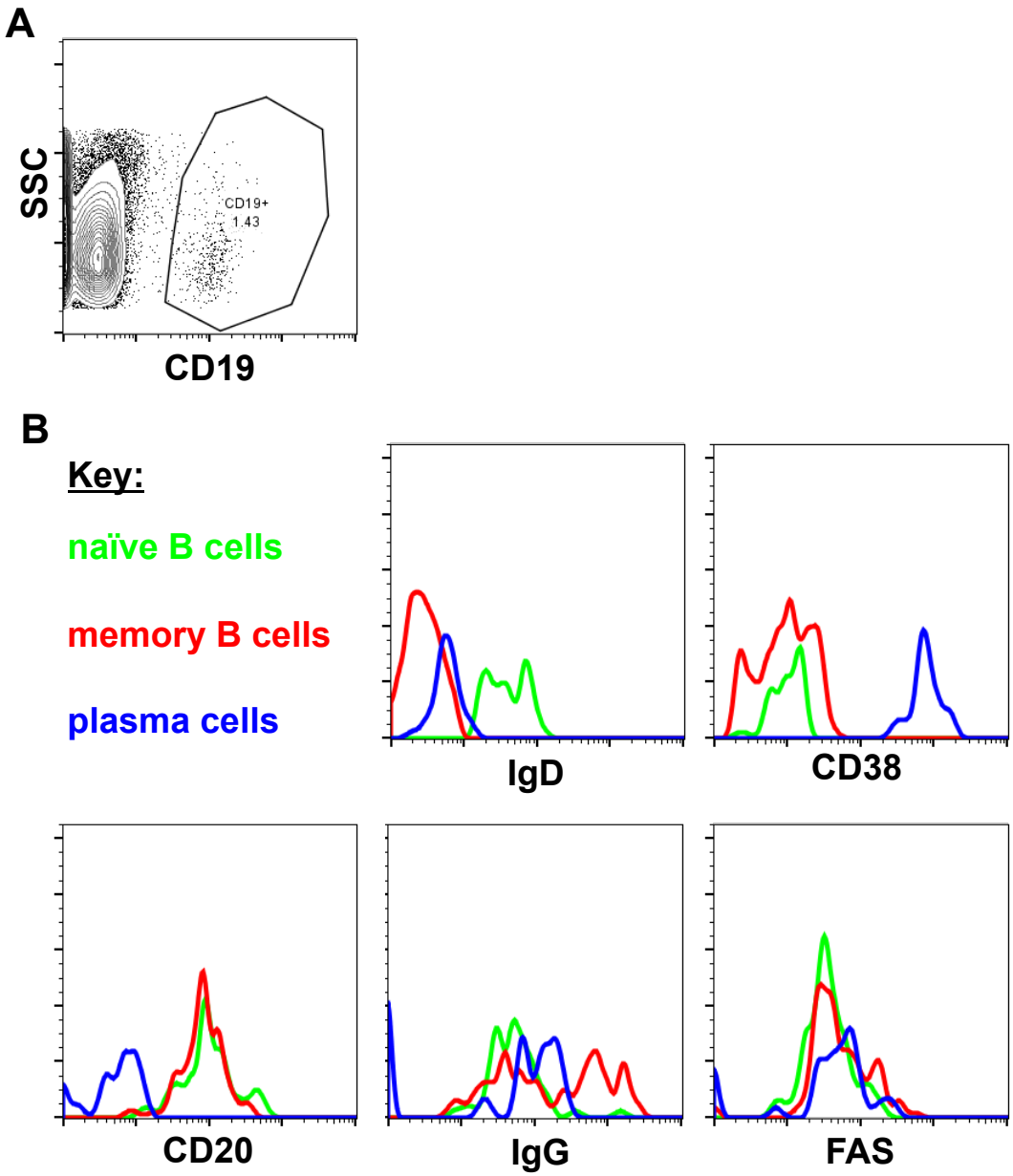

Figure 4. Flow cytometric evidence for early plasma cells in HGSC tumor samples. Physically disaggregated human HGSC tumor preparations were stained with viability dye, and then stained with fluorophore-conjugated antibodies to CD19, CD20, CD38, CD95 (FAS), CD138, IgD, and IgG. After acquisition on an Influx eight-channel flow cytometer, data was analyzed using FloJo software. **A)** CD19+ cells were gated from total viable cells. **B)** Among CD19+ B cells, we identified three main subtypes: naive, memory and plasma cells. Plasma cells exhibited evidence of class switching in that they were IgD- and IgG^{int}. Plasma cells were additionally $CD38^{hi}$, CD20- and FAS+. We did not reliably detect CD138 expression on plasma cells by flow cytometry, similar to other reports.

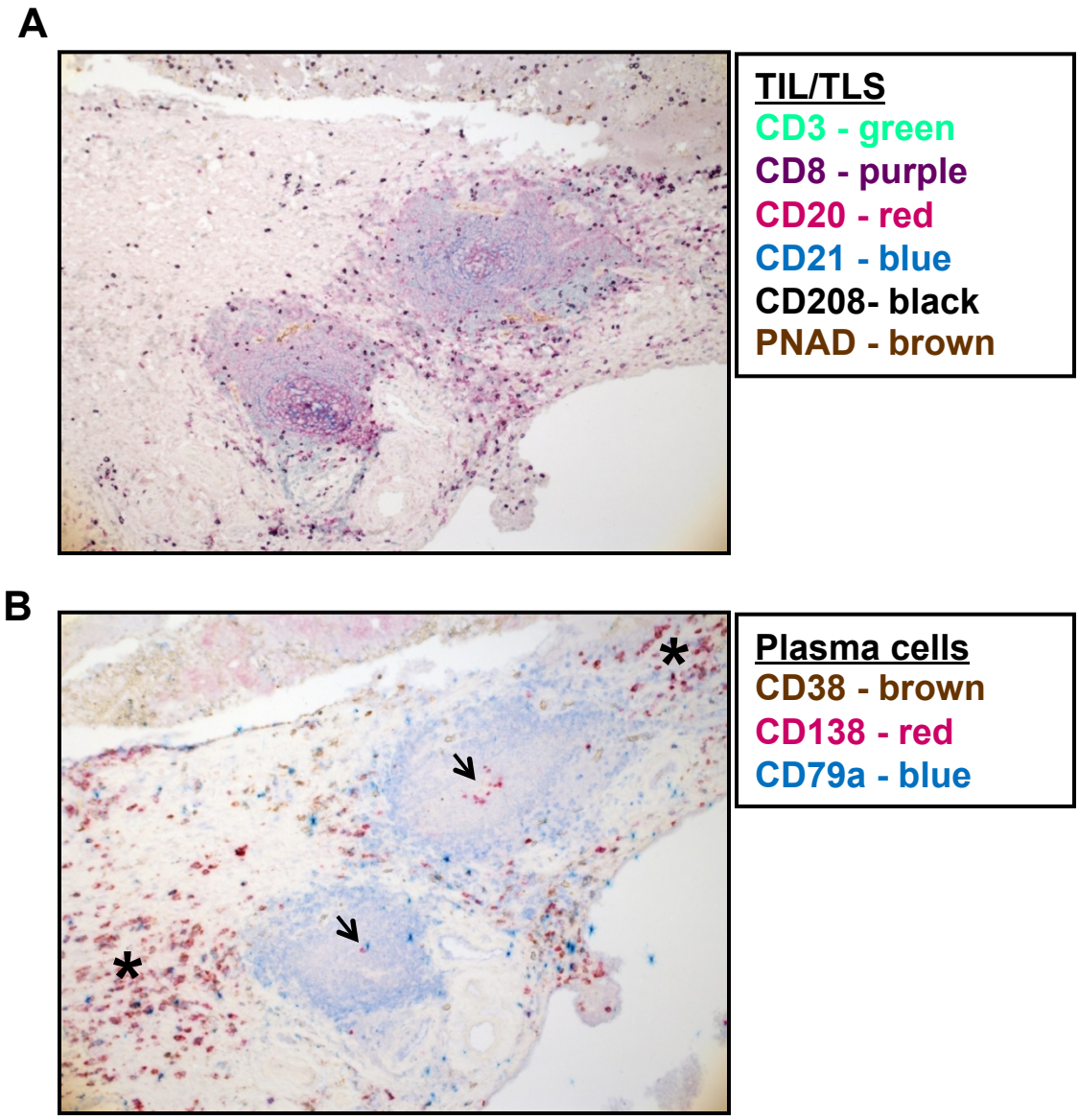

Figure 5. Plasma cells arise within TLS and form dense stromal infiltrates in HGSC. Serial whole tumor sections were stained for the indicated markers. **(A)** Detection of TIL and TLS. TLS appear as aggregates of CD20+ (red) cells containing CD21+ follicular DCs (blue) in germinal centres. **(B)** Plasma cells appear as large cells with CD79a+ (blue) cytoplasm surrounded by double positive CD38+ (brown) and CD138+ (red) membranes. Conventional B cells express CD79a (blue) on the cell membrane. CD138+ cells in germinal centres (indicated by arrows) are thought to be the early plasma cells seen by flow cytometry on the preceding figure. Note also the dense infiltration of tumor stroma by plasma cells (indicated by asterisks) .

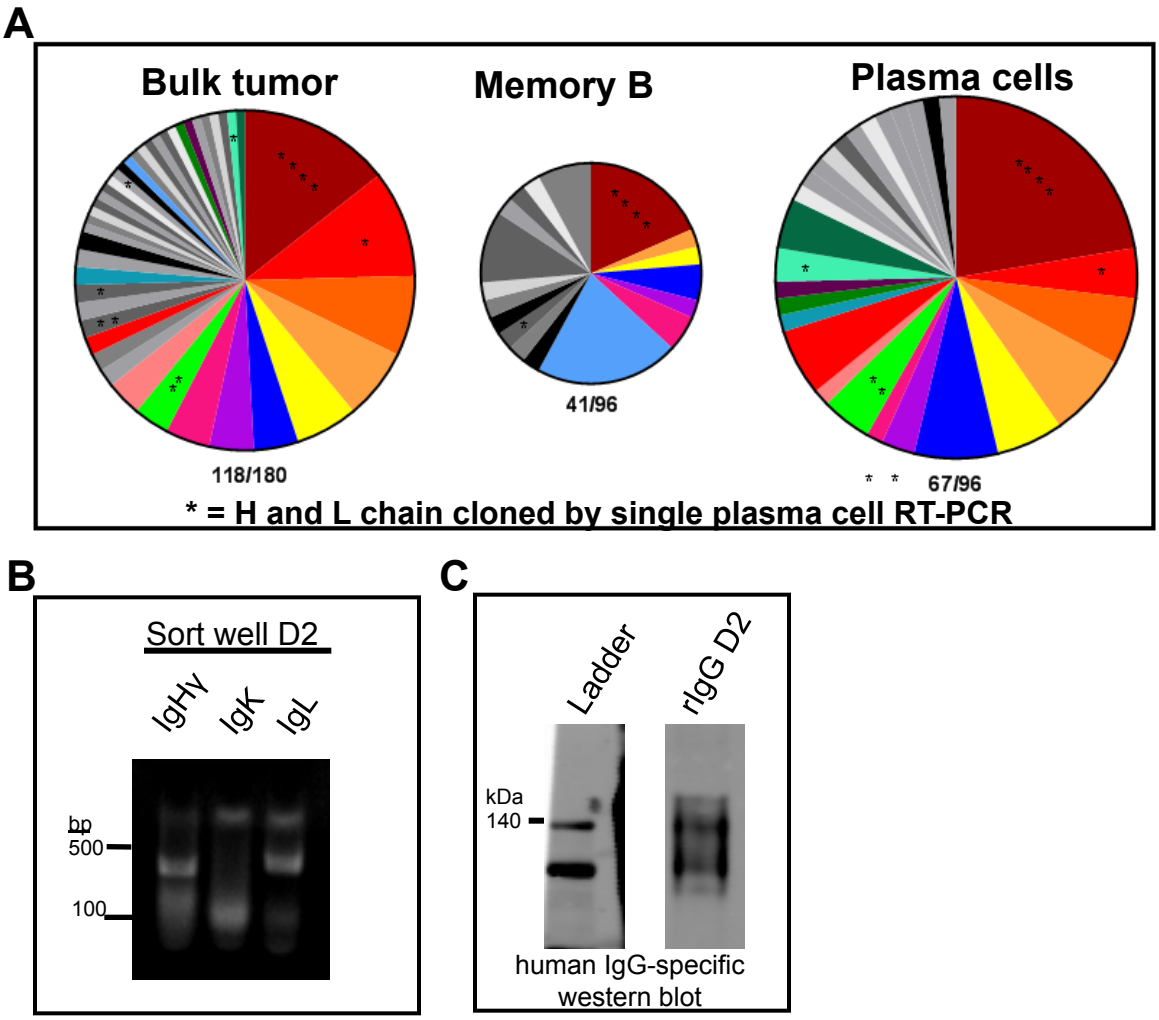

Figure 6. Profiling, cloning and expression of IgG from predominant plasma cell clones in HGSC. (A) Clonal distribution of heavy chain CDR3 sequences as determined by Sanger sequencing variable portions of PCR-amplified IgG from a bulk tumor preparation (left), sorted memory B cells (IgD-, CD38-) (centre), or plasma cells (IgD-, CD38hi) (right) from the same case. Each pie slice represents a unique VDJ rearrangement, and the size of each slice reflects the relative abundance of that CDR3 sequence relative to the total population (also shown by the numbers below each pie). Coloured slices indicate CDR3 sequences that are shared between the 3 compartments. Asterisks indicate VDJ rearrangements for which we have successfully cloned matched heavy and light IgG chains from an individual plasma cell by RT-PCR. **(B)** Single tumor-infiltrating plasma cells (CD19+ CD38hi) were sorted into individual wells of a 96-well plate. Each well was subjected to qRT-PCR with IgG heavy and light chain-specific primers. Shown are PCR products corresponding to immunoglobulin G heavy (IgHγ) (positive), kappa (IgK) (negative), and lambda (IgL) (positive) from one representative plasma cell. **(C)** Human IgG-specific western blot analysis of non-reduced supernatants from 293T cells co-transfected with paired heavy and light chain-encoding expression vectors derived from the same single sorted plasma cell (D2) from (B). Recombinant IgG molecules appear as ~150kDa bands. The protein ladder appears positive due to direct conjugation with fluorescent dye. We have successfully cloned and made rIgG from 15 single plasma cells.

rIg clone	V region	% identity	J region	% identity	D region	CDR3 aa sequence
IROC070 A5 H IROC070 A5 L	IGHV4-59*02 F IGLV2-14*01 F	83.37 94.79	IGHJ3*01/02 F IGLJ2*01 F	78 92.11	IGHD3-10*01 F	CARSRGLITMPSW CSSYSSALYSSSGTLVF
IROC070 B1 H IROC070 B1 K	IGHV3-15*01 F IGKV2-28*01 F	94.24 96.94	IGHJ4*02 F IGKJ3*01 F	93.75 100	IGHD3-10*01 F	CITDVDYYGSGSSWGPHFDYW CMQALQFTF
IROC070 B2 H IROC070 B2 K	IGHV1-3*01 F IGKV3-15*01 F	97.92 99.64	IGHJ4*02 F IGKJ1*01 F	91.67 91.89	IGHD3-3*01	CARGGDDFWSGYRPFDYW CQQYNNWPGTF
IROC070 B5 H IROC070 B5 K	IGHV3-66*01/04 F IGKV1-39*01	94.44 95.34	IGHJ6*02 F IGKJ2*02 F	88.71 88.89	IGHD7-27*01 F	CARDGENKGYYCAMDVW CQQSYTTPRTF
IROC070 B9 H IROC070 B9 K	IGHV3-49*05 F IGVK2-28*01 F	92.86 96.26	IGHJ6*02 F IGKJ5*01 F	82.26 94.44	IGHD3-10*01 F	CVRHYYASEKERRAGQPNYGMDVW CMQALQTPRTF
IROC070 C5H IROC070 C5L	IGHV4-4*02 F IGLV3-21*02F	93.75 92.83	IGJ4*02 F IGL1*01 F	91.67 100	IGHD2-21*02F	CARGGGDSFDLW CQVWDSDTDQNSDQNYVF
IROC070 C10H IROC070 C10K	IGHV3-53 IGKV3-15*01	92.98 96.06	IGJ2*01 F IGKJ4*01 F	92.45 91.67	IGHD2-15*01F	CAKVGSGGACHAGYWYFDLW CQHYDNWLSF
IROC070 D4H IROC070 D4K	IGHV3-15*01 IGKV2-28*01 F	97.28 99.32	IGHJ1*01 F IGKJ1*01F	75 97.22	IGHD6-35*01F	CTTLLMGRIGVATGGW CMQALQTPLTF
IROC070 D6H IROC070 D6K	IGHV3-66*01 F IGKV3-15*01 F	93.33 96.42	IGHJ5*02 IGKJ4*01 F	86.27 97.22	IGHD2-21*01 F	CARRGGDLWWLDLW CQQYNNWPLTF
IROC070 D7H IROC070 D7K	IGHV1-18*01 F IGKV3-11*01F	87.85 95.7	IGHJ4*02 F IGKJ4*01 F	97.92 91.67	IGHD2-8*01	CARLSGPLILYYFDYW CQQRSNWLSF
IROC070 D11H IROC070 D11L	IGHV3-15*01 F IGLV1-47*01	90.82 89.47	IGHJ6*02 F IGLJ3*02F	87.1 91.43	IGHD1-14*01	CTTDGTEPPYQYGMDVW CSTRDDRLRSPEF

Figure 7. Molecular cloning, sequencing, and alignment of paired immunoglobulin genes. Following PCR amplification, pairs of immunoglobulin genes were molecularly cloned into expression vectors. Inserted portions were then sequenced by Sanger sequencing. Following sequencing, the variable portions of cloned immunoglobulin sequences were aligned to the germline elements via the IMGT V-Quest software.

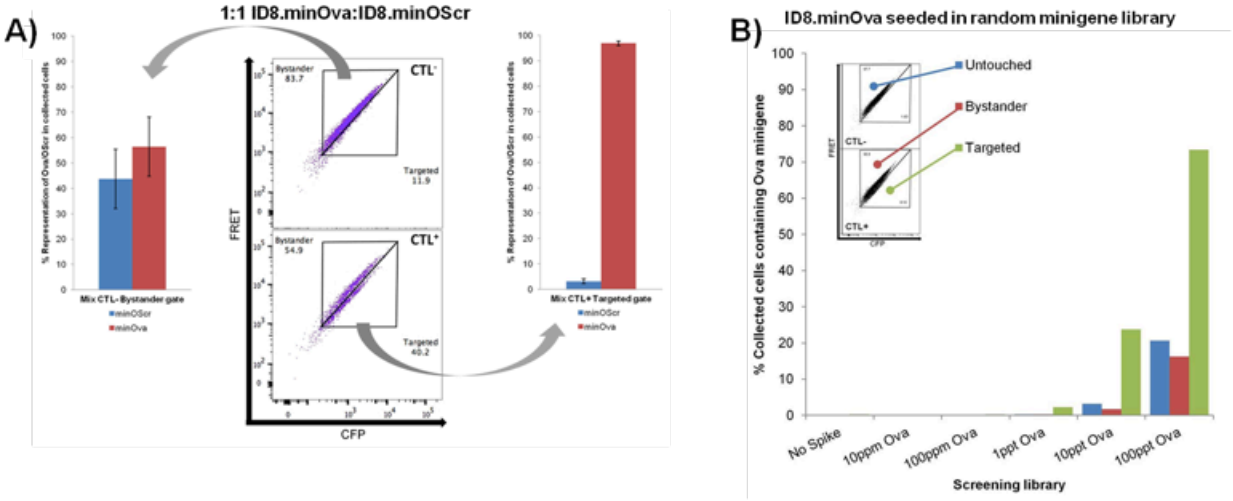

Figure 8. A new high throughput platform for efficient identification of T cell antigens. **(A)** ID8 cells transduced with either the Ova minigene or Ova-scrambled minigene were combined at a 1:1 ratio to form a binary mixed target population. Targets were co-incubated with OT-I CTL for 4h prior to FACS analysis. Recovered cells were lysed and genomic DNA was used as template for qPCR assays using a custom primer/probe set capable of distinguishing between Ova and Ova-scrambled sequences. **(B)** Mixtures of ID8.minOva and ID8.RM were co-incubated with OT-I CTL at a 1:1 target/effector ratio for 4h prior to FACS analysis. Recovered cells were lysed and integrated minigenes were amplified from genomic DNA using PCR primers specific for the conserved transgene region flanking the minigene site. Amplicons were sequenced on the Illumina MiSeq platform with 2x250 paired-end chemistry.

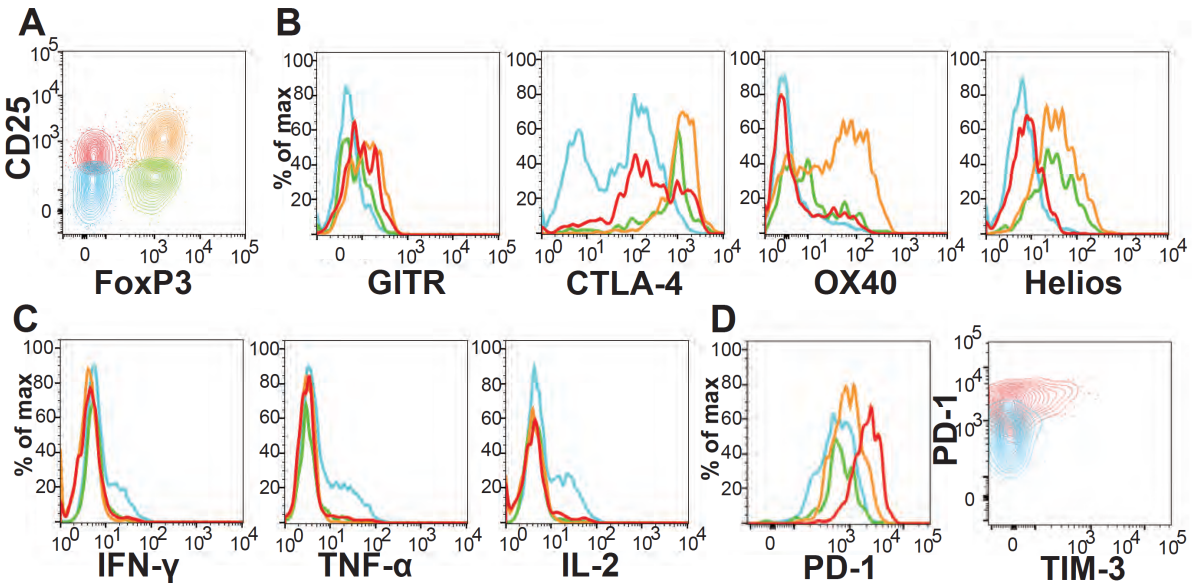

Figure 9. Phenotype and functional characteristics of CD4+ TIL subsets. Multi-parameter flow cytometry was used to assess expression of the indicated activation and differentiation markers and cytokines for four CD4+ T cell subsets defined by CD25 and FoxP3 expression. **(A)** Contour plot showing four CD4+ TIL subsets and color scheme used in other panels: CD25+FoxP3- (red), CD25+FoxP3+ (orange), CD25-FoxP3- (blue), CD25-FoxP3+ (green). **(B)** Expression of T cell activation and differentiation markers by the four TIL subsets. **(C)** Cytokine production after 3 hours of stimulation with PMA and ionomycin. **(D)** Expression of exhaustion markers (note that the right panel shows only the CD25+FoxP3- and CD25-FoxP3- subsets). Data is shown for one representative case from a total of six. Additional information can be found in deLeeuw et al. *Can Imm Res* 2015.

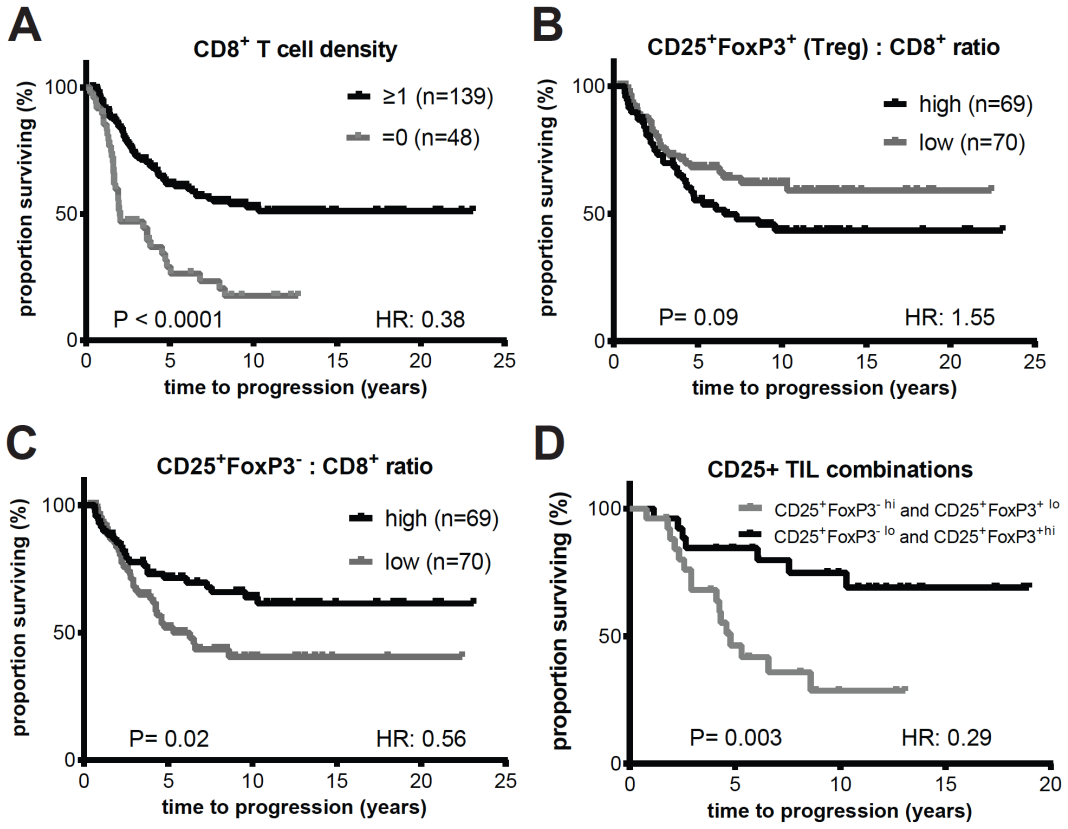

Figure 10. Prognostic significance of TIL subsets. Kaplan-Meier plots showing the association between TIL subsets and progression free-survival in a large HGSC cohort. **(A)** Density of intraepithelial CD8+ TIL. **(B)** Ratio of CD25+FoxP3+ to CD8+ TIL. **(C)** Ratio of CD25-FoxP3+ to CD8+ TIL. **(D)** Ratio of CD25+FoxP3- to CD8+ TIL. In each panel, log-rank tests were used to determine P-values, and hazard ratios (HR) are shown for each analysis. For panels B-D, analyses were restricted to cases that were positive for CD8+ TIL. Additional information can be found in deLeeuw et al. *Can Imm Res* 2015.

Appendix A

Kroeger, D.R., Milne, K., **Nelson, BH** 2015. Plasma cell infiltration identifies ovarian cancers with robust cytolytic T cell responses and superior prognosis. *Under review at Clinical Cancer Research.*

Plasma cell infiltration identifies ovarian cancers with robust cytolytic T cell responses and superior prognosis

Authors:

David R. Kroeger[1], Katy Milne[1], and Brad H. Nelson*[1,2,3]

Affililations:

[1] Deeley Research Centre, British Columbia Cancer Agency, Victoria BC, Canada

[2] Department of Biochemistry and Microbiology, University of Victoria, Victoria BC, Canada

[3] Department of Medical Genetics, University of British Columbia, Vancouver BC, Canada

Running Title: Lymphoid structures, plasma cells, and survival in ovarian cancer

Keywords: B cells, CD8+ T cells, plasma cells, ovarian cancer, immunotherapy

Address correspondence to:

Brad Nelson, Ph.D.
Director and Distinguished Scientist
Deeley Research Centre,
BC Cancer Agency,
2410 Lee Avenue,
Victoria BC, Canada V8R 6V5
Email: bnelson@bccrc.ca
(tel) 1-250-519-5700, (fax) 1-250-519-2040

Funding Sources: Canadian Institutes of Health Research (Award MOP-137133), U.S. Department of Defense (Award W81XWH-12-1-0604), Canadian Cancer Society Research Institute (Award 702497), OVCARE & Vancouver General Hospital Foundation (Carraressi Foundation Research Grant, 2013), and BC Cancer Foundation

Financial Conflicts of Interest: None

Word Count: 4900

Total Number of Figures: 9 (6 + 3 supplementary)

Number of Tables: 6 supplementary

Statement of Translational Relevance:

The role of B cells in anticancer immunity remains controversial. Our data directly addresses this controversy by demonstrating that plasma cells (PCs) are an integral component of robust CD8+ tumor-infiltrating lymphocytes (TIL) responses. We show that the well-established prognostic benefit of CD8+ TIL is restricted to tumors that additionally harbor PCs. Our findings indicate that, rather than working in opposition, the B cell- and T cell-lineages mount closely integrated responses to human tumors as reflected by their physical co-localization, synergistic functional profiles, and interdependent prognostic significance. We discuss the implications of these findings for the development of immunotherapies that engage and fortify intrinsic tumor surveillance mechanisms to achieve more durable clinical responses.

Abstract:

Purpose: CD8+ tumor-infiltrating lymphoyctes (TIL) are key mediators of anti-tumor immunity and are strongly associated with survival in virtually all solid tumors. However, the prognostic effect of CD8+ TIL is markedly higher in the presence of CD20+ B cells, suggesting cooperative interactions between these lymphocyte subsets lead to more potent anti-tumor immunity. **Experimental Design:** We assessed the co-localization patterns, phenotypes, and gene expression profiles of tumor-associated T- and B-lineage cells in high grade serous ovarian cancer (HGSC) by multicolor immunohistochemistry, flow cytometry, and bioinformatic analysis of gene expression data from The Cancer Genome Atlas. **Results:** T cells and B cells co-localized in four types of lymphoid aggregate, ranging from small, diffuse clusters to large, well-organized tertiary lymphoid structures (TLS) resembling activated lymph nodes. TLS were frequently surrounded by dense infiltrates of plasma cells (PCs), which comprised up to 90% of tumor stroma. PCs expressed mature, oligoclonal immunoglobulin G transcripts, indicative of antigen-specific responses. PCs were associated with the highest levels of CD8+, CD4+ and CD20+ TIL, as well as numerous cytotoxicity-related gene products. CD8+ TIL carried prognostic benefit only in the presence of PCs and these other TIL subsets. PCs were independent of mutation load, *BRCA1/2* status, and differentiation antigens but positively associated with cancer-testis antigens. **Conclusions:** PCs are associated with the most robust, prognostically favorable CD8+ TIL responses in HGSC. We propose that TLS facilitate coordinated anti-tumor responses involving the combined actions of cytolytic T cells and antibody-producing PCs.

Introduction:

To mediate effective tumor control, the immune system must contend with the spatial heterogeneity and dynamic evolutionary processes that characterize human cancer. Advanced carcinomas are composed of multiple subclones that, despite a common cellular origin and shared founder mutations, show divergent genetic, biological, clinical, and immunological properties[1]. Moreover, the subclonal structure of cancers continually evolves in response to the selective pressures imposed by the host and the cytotoxic effects of treatment[2]. Tumor evolution can lead to the emergence of treatment-resistant variants that ultimately give rise to fatal disease. Yet at the same time, emerging tumor variants can express novel antigens that instigate new cycles of immune recognition and attack. Thus, for the immune system to successfully contend with advanced cancers, it must deploy surveillance and effector mechanisms that continually adapt to the evolving tumor. Understanding these mechanisms is essential for the development of immunotherapies that yield durable responses.

These concepts are well illustrated by high-grade serous ovarian cancer (HGSC)[3]. At the genomic level, HGSC is characterized by near universal mutations in the tumor suppressor *TP53*, as well as frequent disruption of *BRCA1*, *BRCA2* or other genes involved in homologous DNA repair, resulting in a high degree of genomic instability[4]. Although HGSC has an intermediate mutation load, tumors show extensive copy number variation[4]. Compounding this genomic complexity, HGSC disseminates early and extensively and typically is not detected until advanced stages[3]. As a result, HGSC exhibits a high degree of spatial heterogeneity involving potentially dozens of genomically distinct subclones with extensive dissemination across metastatic sites[5-7]. Although HGSC is highly sensitive to primary platinum-based chemotherapy,

the development of chemo-resistant disease is common and can bring profound changes in subclonal architecture and mutation profiles[6-8].

Despite this complexity, there is a strong link between anti-tumor immunity and patient survival in HGSC, suggesting the immune system can contend with tumor heterogeneity in a substantial proportion of cases. In particular, the presence of CD8+ tumor-infiltrating lymphocytes (TIL) in primary tumors carries a >2-fold increased likelihood of survival[9]. Importantly, however, CD8+ TIL do not operate in isolation. We have shown that tumors containing CD8+ TIL are often additionally infiltrated by CD20+ B cells[10,11]. CD20+ TIL exhibit an antigen-experienced, immunoglobulin G (IgG) positive memory phenotype[11]. Importantly, tumors containing both CD8+ and CD20+ TIL are associated with higher survival rates than those containing CD8+ TIL alone. Similar results have been reported in a variety of other cancers[12-14], suggesting that effective tumor immunity involves cooperative interactions between T cells and B cells.

In our prior study[11], we found that CD8+ and CD20+ TIL often co-localized in lymphoid aggregates of various sizes and morphology. This is reminiscent of autoimmune conditions, where lymphoid aggregates develop in affected tissues. In rheumatoid arthritis, lymphoid aggregates have been classified into three grades ranging from small perivascular collections of B and T cells (grade 1) to large, highly organized structures resembling lymph nodes (grade 3)[15]. These latter aggregates, referred to as tertiary lymphoid structures (TLS), are found not only in autoimmunity, but also in chronic infection, graft rejection, and cancer[16]. Like conventional lymph nodes, TLS harbor prominent B cell follicles adjoined by discrete T cell zones containing CD4+ and CD8+ T cells, DC, and high endothelial venules (HEV)[16]. The B cell follicles of active TLS contain germinal centers (GC) with interdigitating networks of follicular dendritic

cells (fDC). In the setting of cancer, TLS are receiving increased attention, as they have been associated with favorable prognosis in several solid tumors[17-19].

To better understand the mechanisms by which T cells and B cells work together to mediate anti-tumor immunity, we investigated the co-localization patterns, phenotypes, and gene expression profiles of tumor-associated T- and B-lineage cells in HGSC. We found that the most robust, prognostically favorable CD8+ TIL responses are accompanied not only by CD20+ TIL but by dense stromal infiltrates of IgG+ plasma cells. We propose that optimal anti-tumor immunity may involve closely integrated cytolytic- and antibody-mediated effector mechanisms.

Materials and Methods:

Additional information is provided in Supplementary Materials.

Patient cohorts

The study protocol was approved by the Research Ethics Board of the BC Cancer Agency (BCCA) and University of British Columbia (Vancouver BC). HGSC tumor specimens were obtained from previously untreated patients from a prospective cohort (treated between 2007-present) or retrospective cohort (optimally de-bulked cases treated between 1984-2000; **Table S4**) [10,20]. Bioinformatic analyses utilized the HGSC dataset from The Cancer Genome Atlas [4].

Immunohistochemistry (IHC) and image analysis

Antibodies are listed in Table S6. Multicolor IHC of formalin-fixed paraffin-embedded (FFPE) tissue was performed using previously described methods[11]. Slides were scanned with an Aperio ScanScope (Leica Biosystems, Wetzlar Germany) and analyzed using ImageScope software v12.1 (Aperio Technologies, Vista CA) with the Stereology Toolkit v4.2.0 (ADCIS,

Saint-Contest, France). TIL were enumerated in ten random 20x fields, and cell counts were normalized to the area of tumor epithelium evaluated. PC density was measured using a four-point scale[21]; for survival analyses, cases with PC scores $\geq$1 were deemed positive.

Flow cytometry

Disaggregated tumor cell suspensions were washed and labeled with fluorophore-conjugated monoclonal antibodies (**Table S6**). Flow cytometry and sorting were performed using a BD Influx instrument (Mississauga ON).

IgG sequence analysis

RNA was extracted from FACS-purified memory B cells and plasma cells (1-5 $x10^3$ each) and bulk tumor cells (2.5 x 10^6). PCR reactions were performed using primers designed to amplify all *IGHG* variable regions. Up to 192 clones per sample were subjected to Sanger sequencing.

NanoString gene expression analysis

Total RNA was prepared from FFPE whole tumor sections using the AllPrep DNA/RNA FFPE kit (Ambion, Life Technologies, Carlsbad CA). Total RNA (200 ng) was analyzed using the Pan Cancer Immune Profiling panel and nCounter platform (NanoString Technologies, Seattle WA). Data was normalized using nSolver software.

Bioinformatic analysis

The HGSC gene expression array dataset from The Cancer Genome Atlas (TCGA) was downloaded from bioconductor.org. Corresponding RNA-seq data, non-synonymous point mutation counts, *BRCA1*, *BRCA2*, and *TP53* mutation status, and *BRCA1* promotor methylation calls were appended.

Statistical analysis

Statistical analyses were performed using R v3.1.1 and GraphPad Prism v6.0. *P*-values of less than 0.05 were considered significant unless otherwise stated.

Results

Multicolor IHC reveals four types of lymphoid aggregate in HGSC

To visualize the different lymphoid aggregates present in HGSC, we developed a 6-color IHC panel that enabled simultaneous detection of CD8+ and CD4+ (CD3+CD8-) T cells, CD20+ B cells, CD21+ follicular DC (fDC), CD208+ activated conventional DC (DC), and PNAd+ HEV-like vessels. The panel was applied to whole sections from 30 randomly selected HGSC tumors. To control for anatomical location, we stained an equal number of specimens from ovary or omentum; for 7 cases, we stained matched ovary and omentum samples to allow direct comparison between these sites.

We observed a variety of lymphoid aggregates, which we classified into four types based on size, cellular composition, and degree of organization. *Type 1* aggregates were small (approximately 20 to 50 cells), compact, and composed of CD4+ and CD8+ T cells, B cells, and occasional DC **(Fig. 1A)**, thereby resembling grade 1 aggregates in RA[15]. *Type 2* aggregates were larger (100 to >1000 cells) and composed of CD4+ and CD8+ T cells and CD20+ B cells **(Fig. 1B)**. These aggregates were diffuse and lacked discrete zones or follicles. *Type 3* aggregates represented fully developed TLS, similar to grade 3 aggregates in RA[15]. TLS had prominent B cell follicles with germinal center (GC)-like structures characterized by interdigitating networks of CD21+ fDC. In addition, they contained discrete T cell zones with CD4+ and CD8+ T cells, DC, and PNAd+ HEV-like vessels **(Fig. 1C)**. Finally, *Type 4* aggregates were composed of approximately 100-300 CD20+ B cells and fDC organized into follicles with few CD4+ and CD8+ T cells (**Fig. 1D**). As these structures did not contain clear T cell zones and were primarily (6/7) found in omental samples, we speculated many or all were normal milky spots[22].

The four types of aggregate were strongly associated with one another. Type 1 and 2 aggregates were found in the same 17/30 tumors, and indeed might represent a continuum of structures. TLS were found in 7/30 tumors, all of which contained Type 1 and 2 aggregates. Type 4 aggregates were observed in 7/30 tumors, of which 7/7 contained Type 1 and 2 aggregates and 5/7 contained TLS. Type 1 and 2 aggregates were more prevalent in omental (11/23) versus ovarian (6/23) samples. Likewise, TLS were present in 5/23 omental versus 2/23 ovarian samples. However, none of these differences reached statistical significance.

All four types of aggregate were strongly associated with TIL. Tumors containing Type 1 or 2 aggregates were positive for CD4+ and CD8+ TIL in 17/17 cases and CD20+ TIL in 14/17 cases. Likewise, all tumors containing TLS (7/7) contained CD4+, CD8+, and CD20+ TIL (**Fig. 1E**). We compared the density of TIL in TLS-proximal (<500 μm from the TLS center) versus TLS-distal (>500 μm) tumor regions. CD20+ TIL showed a >10-fold greater density in TLS-proximal epithelium (28.5 vs. 2.5 cells/20x field; P= 0.013, Mann-Whitney test; **Fig. 1F**). CD4+ and CD8+ TIL showed a similar trend (72 vs. 24 and 227 vs. 59 cells/20x field, respectively), although this did not reach statistical significance (**Fig. 1F**). TIL densities were similar between omental and ovarian sites (all $P > 0.4$, Mann-Whitney test).

TLS are associated with dense plasma cell infiltrates in tumor stroma

To investigate whether the GC-like structures observed in TLS were sites of B cell differentiation, sections containing TLS were subjected to three-color IHC with antibodies to BCL-6, CD3 and CD20. We detected nuclear expression of BCL-6 in both CD20+ and CD3+ cells within B cell follicles, indicating the presence of GC B cells and Tfh, respectively (**Fig. 2A**). Moreover, virtually all TLS contained AID+ CD20+ B cells, which are indicative of

ongoing immunoglobulin class switching and somatic hypermutation (**Fig. 2B**). BCL-6+ and AID+ B cells were also observed in Type 4 aggregates but not Type 1 or 2 aggregates. Thus, TLS exhibited the hallmarks of ongoing GC reactions.

Tumors were stained with antibodies to CD38, CD138 and CD79a to distinguish PCs (which are CD20- but co-express CD38, CD138, and cytosolic CD79a) from naive and memory B cells (which are CD38-CD138- but express membranous CD79a) and CD138+ tumor or stromal cells. PCs were found in 21/30 of tumors and generally formed dense stromal infiltrates, constituting 50-90% of stromal cells (**Figs. 2C, D**). PCs were typically concentrated near the periphery of TLS (**Fig. 2E**). In several cases, CD138+ cells were observed in GCs (**Fig. 2F**). There was a strong association between TLS and the density of stromal PCs (mean PC score in the presence of TLS = 2.6 vs. 1.0 in the absence of TLS, $P = 0.0004$, Mann-Whitney test; **Fig. 2G**), although 2/30 tumors contained abundant PCs (PC score of 3) in the absence of TLS (**Fig. 2G**). Thus, TLS-associated GCs could serve as sites of PC differentiation. The density of PCs was also positively associated with the intraepithelial density of CD4+, CD8+, and CD20+ TIL (all Spearman's r >0.6, $P < 0.001$; **Fig. 2F**).

Tumor-associated PCs are IgG+CXCR3+ and clonally expanded

The phenotype of PCs was further defined by flow cytometry of disaggregated viable tumor samples from 12 of the above cases. The proportion of CD19+ B cells varied widely between tumors (mean = 6.1% of viable lymphocytes; range = 0.4-30). Based on the surface expression of IgD and CD38, we identified three major CD19+ lymphocyte subsets: IgD+IgG-CD38- naive B cells, IgD-IgG+CD38- memory B cells, and IgD-IgG+CD38+ PCs (**Fig. 3A**). As shown previously[11], the majority of memory B cells were IgG positive (**Fig. 3B**). PCs comprised

from 5-88% of CD19+ cells and also expressed surface IgG (**Fig. 3B**). As in the IHC analysis, there was a trend towards larger proportions of PCs in tumors containing TLS (mean proportion of CD19+ cells: 39% vs. 25%), although 2/12 tumors had abundant PCs (>30% of CD19+ cells) despite lacking TLS.

CD19+ cells were further assessed for expression of B cell differentiation markers. As expected, naive B cells were CD20+CD27-CD95-CD138-, and memory B cells were CD20+CD27+CD95+CD138- (**Fig. 3C**). Also as expected, PCs were CD20-CD27+CD95+ and showed low but consistent expression of CD138 (**Fig. 3C**). The chemokine receptors CXCR5 and CXCR3 recruit B-lineage cells into follicles and sites of inflammation, respectively. As expected, naive B cells expressed CXCR5 but not CXCR3, whereas the memory B cell population was a mixture of CXCR5+ and CXCR3+ cells (**Fig. 3C**). In contrast, PCs universally expressed CXCR3 but not CXCR5. Thus, PCs appeared to be at an early stage of differentiation and had an inflammatory chemokine receptor profile.

To assess clonality, we FACS-purified PCs from 3 tumors and sequenced the Ig heavy-chainvariable regions. Bulk tumor samples and FACS-purified memory B cells were analyzed for comparison. In 3/3 tumors, PC-derived sequences were restricted to 10-28 distinct *VDJ* families (**Fig. 3D, Table S1**), suggesting a high degree of clonal expansion. There was also widespread evidence of somatic hypermutation within *VDJ* families, with most sequences showing at least 5% divergence from germline. Although CDR3 sequences from PCs and memory B cells showed some overlap, PC-derived sequences were most similar to those from bulk tumor in terms of both diversity and prevalence (**Fig. 3D**). Thus, PCs were clonally expanded and represented the predominant source of IgG mRNA in tumors.

A coordinated antitumor response including PCs is associated with survival in HGSC

To assess the prognostic significance of tumor-associated PCs, we analyzed a retrospective HGSC tissue microarray which has been previously evaluated for numerous TIL subsets[10,11,23]. PCs were detected with antibodies to CD138 and CD79a, as our previous analysis showed that CD79a+CD138+ PCs universally expressed CD38 (**Fig. 2D, 3A**). Consistent with our initial IHC analysis, PCs were found in 36% (62/172) of cases and showed a predominantly stromal location. When PCs were considered in relation to other TIL subsets, 90% of cases (155/172) fell into one of six subgroups: **(a)** no TIL (11% of cases); **(b)** CD8+ TIL alone (7.5%); **(c)** CD8+ and CD4+ TIL (20%); **(d)** CD8+ and CD4+ TIL with PCs (13%); **(e)** CD8+, CD4+ and CD20+ TIL (16%); and **(f)** CD8+, CD4+ and CD20+ TIL with PCs (23%) (**Fig. 4A**). These subgroups showed no association with patient age or stage of disease (ANOVA P=0.777, chi-squared P=0.6173, respectively).

The six subgroups carried distinct prognostic significance (**Fig. 4B**). The survival rate associated with CD8+ TIL alone was similar to tumors lacking TIL altogether. Of tumors containing CD8+ TIL, those that additionally contained CD4+ TIL, CD20+ TIL or PCs were associated with minor, statistically insignificant increases in survival. However, tumors containing CD8+, CD4+ and CD20+ TIL together with PCs were associated with markedly increased survival, with approximately 65% of patients alive at 10 years. Thus, the prognostic benefit of TIL in HGSC is associated with the combination of these four lymphocyte subsets.

Identification of a minimal plasma cell gene expression signature

To investigate the relationship between PCs and the underlying molecular and genetic features of HGSC, we sought to identify a PC-associated gene expression signature that could be used to interrogate the TCGA dataset. We assessed the expression of 770 cancer/immune-related genes in 19 HGSC samples that, in the above IHC analyses, were found to be (a) positive for both PCs and CD20+ B cells (n=10), (b) positive for PCs but negative for CD20+ B cells (n=4), (c) negative for PCs but positive for CD20+ B cells (n=2), and (d) negative for both PCs and CD20+ B cells (n=3). All tumors contained CD4+ and CD8+ TIL. Average transcript counts between the 4 subgroups were highly concordant (**Fig 5A**; Pearson $r^2 > 0.85$). However, 66 genes were expressed at >10-fold higher levels in PC high tumors (PC score of 3; n=4) (**Table S2**), including the B-lineage genes *CD79A, MS4A1* (CD20) and *TNFRSF17* (B cell maturation antigen; BCMA) (**Fig. 5A**). Of these, expression of *TNFRSF17* was uniquely associated with PC positive tumors compared to tumors containing B cells but not PCs, or the other subgroups of tumors (**Table S2**). TNFRSF17/BCMA is known to be expressed when B cells differentiate into antibody-secreting cells[24], and it is essential for the survival of long-lived PCs but not memory B cells[25]. Moreover, *TNFRSF17* has been described as a signature gene for human PCs[26].

Given our observation that PCs contribute the majority of IgG mRNA in HGSC tumors (**Fig. 3D**), we reasoned that *TNFRSF17* and IgG gene expression levels should be correlated. Indeed, analysis of TCGA[27] microarray data revealed a strong correlation between the expression of *TNFRSF17* and the immunoglobulin joining region (*IGJ*) gene segment, which is common to all antibody mRNA transcripts (Spearman's r = 0.86; Pearson's $r^2 = 0.81$). When we plotted normalized gene expression values for these two genes, three patient subgroups emerged (**Fig. 5B**): **(a)** high expression of both *TNFRSF17* and *IGJ* (n=56), **(b)** moderate to high expression of *IGJ* but not *TNFRSF17* (n=313), and **(c)** negligible expression of *TNFRSF17* and *IGJ* (n=201). A

similar pattern was seen using RNA-seq data from a subset of these tumors (**Fig. 5C**). As expected, tumors that expressed both *TNFRSF17* and *IGJ* also expressed high levels of *IGHV* segments (**Fig. 5D**). The majority of such cases expressed 5-15 *IGVH* segments (**Fig. 5D**), consistent with the oligoclonal nature of IgG transcripts we observed by Sanger sequencing of *IGHV* regions (**Fig. 3D**). Finally, in accord with our flow cytometry data (**Fig. 3B**), IgG-derived transcripts were far more abundant than other immunoglobulin subtypes. Specifically, *IGG1*, *IGG2*, and *IGG3* were predominant, with low expression of *IGG4*, *IGA1*, and *IGM* in some cases (**Fig. S1**). Thus, *TNFRSF17* and *IGJ* comprised a two-gene signature that distinguished TCGA cases with **(a)** both PCs and CD20+ TIL ($TNFRSF17^{high}$ and IGJ^{high}); **(b)** CD20+ TIL without PCs ($TNFRSF17^{low}$ and IGJ^{high}); and **(c)** neither CD20+ TIL nor PCs ($TNFRSF17^{low}$ and IGJ^{low}).

Association of the PC signature with immune-related genes, patient survival, and CT antigens

The *TNFRSF17*/*IGJ* gene signature was used to explore associations between PCs and other immune-related gene products in the TCGA gene expression microarray dataset. Consistent with our IHC data (**Fig. 2E**), tumors with a PC signature (i.e., $TNFRSF17^{high}$ and IGJ^{high}) showed elevated expression of *CXCL13* (which contributes to the establishment and organization of TLS) and *IL21* (which is produced primarily by Tfh cells) (**Fig. 6A**). Although a marker of TLS, CXCL13 is unlikely to serve as a chemoattractant for PCs, as PCs express the inflammation-associated chemokine receptor CXCR3 rather than CXCR5 (**Fig. 3C**)[28]. Indeed, the three CXCR3 ligands (*CXCL9, CXCL10* and *CXCL11*) were highly expressed in tumors with PC or B cell signatures (**Fig. 6B**), providing a plausible mechanism for attraction of PCs to the tumor microenvironment. Tumors with a PC signature also showed high expression of *TNFSF13B* (BAFF, a ligand for BCMA) (**Fig. 6C**). In contrast, *IL6* levels were only modestly elevated, and

TNFSF13 (APRIL) and *CXCL12* levels were similar to the PC-negative subgroups (**Fig. 6C**). Thus, the BAFF/BCMA axis might provide the primary growth and survival signal for PCs in the HGSC microenvironment.

We also evaluated the relationship between PCs, cytolytic gene signatures, and prognosis. Consistent with our IHC data (**Fig. 2H**) we observed a stepwise increase in the expression of *CD8A* (a marker of CD8+ TIL) in cases with B cell and PC signatures (**Fig. 6D**), whereas expression of the Treg-associated transcription factor *FOXP3* was uniform across subgroups (**Fig. 6E**). Cases with the PC gene signature also showed elevated expression of *IFNG*, *GZMB*, and *PRF1* (**Fig. 6F**). In accord with this cytotoxic T cell signature, the PC gene signature was strongly associated with overall survival (no B cells vs. PC, log-rank *P*=0.0086; B cells vs. PC *P*=0.0241), whereas *IGJ* alone carried no prognostic benefit (**Fig. 6G**). Thus, consistent with our IHC data (**Fig. 4B**), PCs were associated with cytotoxic immune responses and patient survival.

To gain insight into potential target antigens of PCs, we evaluated the relationship between the PC gene signature and various classes of tumor antigen. Non-synonymous point mutations can give rise to "neo-epitopes" that are recognized by CD8+ and CD4+ TIL[29]. However, neither the PC nor B cell gene signatures showed an association with the total number of point mutations in tumors (chi-squared P=0.9429; **Fig. 6H**) nor predicted HLA-A associated neo-epitopes (chi-squared *P*=0.7675; **Fig S2A**). Although *BRCA1* impairment has been correlated with the expression of TIL-related genes in HGSC[30,31], the PC and B cell gene signatures showed no association with *BRCA1* impairment (including germline mutations, somatic mutations and DNA methylation) (Chi-squared *P*=0.7415; **Fig. 6I)** nor *BRCA2* mutation (Chi-squared *P*=0.9142). Likewise, the PC and B cell gene signatures were not associated with specific types of *TP53* mutation (chi-squared *P*=0.7175; **Fig. S2B**). We also evaluated the

expression of 45 commonly overexpressed antigens and 15 well-characterized differentiation antigens (**Table S3**) but found no association with the PC or B cell gene signatures (**Fig. S2C**). Finally, we assessed the expression of 104 cancer-testis (CT) antigens. Tumors with a PC signature expressed two-fold more CT antigens on average than tumors with a B cell signature or no B cell signature (cut-off: z=3, ANOVA P=0.0003; **Fig. 6J**). Similar results were obtained using different thresholds for gene expression (z=2, P=0.0093 and z=4, P<0.0001). Semi-supervised hierarchical clustering revealed a subset of CT antigens that were over-represented in cases with a PC gene signature (**Fig. S3**), including known targets of autoantibody responses such as NY-ESO-1, MAGE A1 and CTAG2 (**Fig. S3; Table S4**). Thus, from this broad bioinformatic analysis, CT antigens emerged as a potential class of target antigen underlying PC responses in HGSC.

Discussion:

While investigating lymphoid aggregates in HGSC, we discovered a novel, prognostically significant association between TIL, TLS, and PCs. PCs were strongly associated with mature TLS and formed dense aggregates in tumor stroma. PCs had an early differentiated phenotype, expressed surface IgG, and showed evidence of clonal expansion and somatic hypermutation. PC infiltrates were strongly associated with CD8+ TIL and other hallmarks of cytotoxic immune responses. Indeed, CD8+ TIL carried prognostic benefit only when found in combination with PCs, CD20+ TIL and CD4+ TIL, suggesting these four lymphocyte subsets work in concert to promote antitumor immunity. Interrogation of the TCGA dataset revealed correlations between PCs and other features of active antitumor responses, including B-lymphoid growth and survival factors, TLS-associated genes, and cytokines and chemokines associated

with cytolytic immune responses. Tumors with a PC gene signature had average mutation loads and *BRCA1/2* status but expressed more CT antigens, suggesting the latter represent target antigens for PC responses. Collectively, our findings reveal an important but underappreciated collaboration between PCs and TIL in anti-tumor immunity. With better understanding, it may be possible to enhance these functional interactions to achieve improved tumor surveillance and more durable responses to immunotherapy.

The positive associations we found between PCs and tumor immunity are consistent with some but not all prior reports concerning the immunological role of PCs. On the positive side, PCs or PC-like gene signatures have been associated with favorable prognosis in breast[14], lung[21], colorectal[12] and other cancers[13]. Indeed, in a recent pan-cancer gene expression analysis, a PC-associated gene signature was among the strongest positive prognostic factors across cancer types[26]. Moreover, prognostically favorable "B cell" gene signatures often contain immunoglobulin transcripts[14,32], which our data indicates are likely attributable to PCs (**Fig. 3D**). On the other hand, both B cells[33,34] and PCs have been shown to play inhibitory roles in cancer and other settings. Recent studies in infection and autoimmunity have identified a subset of PCs ("regulatory" PCs) that inhibit T cell responses via the immunosuppressive cytokines IL-10 and IL-35[35]. Shalapour and colleagues recently described a similar PC subset in murine and human prostate cancer that inhibited CD8+ T cell-mediated tumor immunity and consequently the effectiveness of chemotherapy[36]. Notably, this PC subset expressed IgA, IL-10 and PD-L1 and differentiated in response to TGF-beta. In contrast, we found that PCs in HGSC universally expressed IgG (**Figs. 3B, S1**), suggesting they undergo class switching in a pro-immune milieu dominated by cytokines such as IFN-γ rather than TGF-β. Moreover, HGSC-associated PCs expressed CXCR3 (**Fig**. **3C**), which is induced in B-lineage cells by an IFN-γ/T-bet dependent

pathway and enables their recruitment to inflammatory sites[37]. CXCR3+ PCs have also been described in autoimmunity[38,39], where they serve to exacerbate rather than suppress immune responses. Thus, the immunosuppressive PCs described in prostate cancer[36] may be unique to that disease, as the PCs found in HGSC and other malignancies have properties and associations consistent with a positive role in anti-tumor immunity.

Given the strong prognostic significance of CD8+ TIL, it is widely assumed that they are the primary mediators of anti-tumor immunity. However, CD8+ TIL are often functionally impaired in the tumor microenvironment[40], raising the possibility that alternative immune mechanisms are equally if not more important. As the normal physiological role of PCs is to serve as "antibody factories", they could mediate anti-tumor effects by producing antibodies against tumor-associated antigens. Such effects might be augmented by the dense localization of PCs in tumor stroma, which would enable high concentrations of antibody to accumulate locally. Theoretically, PC-derived antibodies could mediate direct antitumor effects by binding to and disrupting the function of their cognate antigens, activating the complement pathway, and/or triggering antibody-dependent cellular cytotoxicity (ADCC)[41]. In this regard, the predominant antibody subtypes in HGSC included IgG1 and IgG3 (**Fig. S1**), which can activate both complement and ADCC[41]. Finally, PC-derived antibodies could opsonize tumor antigens, thereby facilitating antigen presentation and broadening of T cell responses[42].

Defining the anti-tumor mechanisms used by PCs will require identification of their cognate antigens. Our bioinformatic analyses suggest that PC-derived antibodies preferentially recognize CT antigens over differentiation/overexpressed antigens or mutant gene products **(Figs. 7, S2)**. Accordingly, Germain and colleagues recently demonstrated recognition of multiple CT antigens by lung cancer-associated antibodies[43]. Other classes of antigen might also

be relevant, as lung cancer-derived antibodies were shown to recognize p53 and various overexpressed self-antigens[44]. Furthermore, antibodies derived from medullary breast cancer were shown to recognize ganglioside D3 and an apoptosis-associated form of actin[45,46]. To better understand the effector mechanisms used by PCs in HGSC, we are cloning IgG molecules from individual PCs and attempting to identify their cognate antigens.

In addition to antibodies, PCs could influence anti-tumor immunity through cell-based mechanisms. PCs can regulate T cell responses by expressing cytokines and other immunomodulatory factors[35]. Another possibility is that PCs might physically exclude immune-suppressive cell types, such as cancer-associated fibroblasts and myeloid-derived suppressor cells[47], creating a more permissive tumor microenvironment for CD8+ TIL responses. Indeed, lymphocyte- and mesenchymal-derived gene signatures are inversely correlated in HGSC[4,30].

Our findings suggest several novel avenues for cancer immunotherapy. The antibody-mediated effects of PCs could potentially be mimicked through administration of recombinant antibodies combined with immune modulators that enhance downstream processes such as antigen spreading, CDC and ADCC. The cell-mediated effects of PCs could potentially be reproduced by adoptive transfer of tumor-specific PCs; induction of TLS using vectors that express relevant cytokines/chemokines[48]; or therapeutic vaccination[49,50]. By designing immunotherapies that engage both the humoral and cellular arms of the immune system, it should be possible to establish endogenous tumor surveillance mechanisms that more effectively contend with the spatial heterogeneity and continual evolution of advanced cancers.

Acknowledgements: We thank Scott Brown and Dr. Rob Holt for bioinformatic assistance.

Author contributions: DRK – Conceived and designed experiments, performed experiments, performed IHC quantitations and analysis of gene expression data, made the figures, wrote and revised the manuscript. KM – performed multicolour immunohistochemistry, reviewed manuscript. BHN – Conceived and designed experiments, wrote and revised the manuscript.

References:

1 Tabassum, D. P. & Polyak, K. Tumorigenesis: it takes a village. *Nat Rev Cancer* **15**, 473-483, doi:10.1038/nrc3971 (2015).

2 Pribluda, A., de la Cruz, C. C. & Jackson, E. L. Intratumoral Heterogeneity: From Diversity Comes Resistance. *Clin Cancer Res* **21**, 2916-2923, doi:10.1158/1078-0432.CCR-14-1213 (2015).

3 Bowtell, D. D. *et al.* Rethinking ovarian cancer II: reducing mortality from high-grade serous ovarian cancer. *Nat Rev Cancer* **15**, 668-679, doi:10.1038/nrc4019 (2015).

4 TCGA. Integrated genomic analyses of ovarian carcinoma. *Nature* **474**, 609-615, doi:nature10166 [pii]
10.1038/nature10166 (2011).

5 Bashashati, A. *et al.* Distinct evolutionary trajectories of primary high-grade serous ovarian cancers revealed through spatial mutational profiling. *J Pathol* **231**, 21-34, doi:10.1002/path.4230 (2013).

6 Schwarz, R. F. *et al.* Spatial and temporal heterogeneity in high-grade serous ovarian cancer: a phylogenetic analysis. *PLoS Med* **12**, e1001789, doi:10.1371/journal.pmed.1001789 (2015).

7 Patch, A. M. *et al.* Whole-genome characterization of chemoresistant ovarian cancer. *Nature* **521**, 489-494, doi:10.1038/nature14410 (2015).

8 Castellarin, M. *et al.* Clonal evolution of high-grade serous ovarian carcinoma from primary to recurrent disease. *J Pathol*, doi:10.1002/path.4105 (2012).

9 Hwang, W. T., Adams, S. F., Tahirovic, E., Hagemann, I. S. & Coukos, G. Prognostic significance of tumor-infiltrating T cells in ovarian cancer: a meta-analysis. *Gynecol Oncol* **124**, 192-198, doi:10.1016/j.ygyno.2011.09.039 (2012).

10 Milne, K. *et al.* Systematic analysis of immune infiltrates in high-grade serous ovarian cancer reveals CD20, FoxP3 and TIA-1 as positive prognostic factors. *PLoS One* **4**, e6412, doi:10.1371/journal.pone.0006412 (2009).

11 Nielsen, J. S. *et al.* CD20+ tumor-infiltrating lymphocytes have an atypical CD27- memory phenotype and together with CD8+ T cells promote favorable prognosis in ovarian cancer. *Clin Cancer Res* **18**, 3281-3292, doi:1078-0432.CCR-12-0234 [pii]
10.1158/1078-0432.CCR-12-0234 (2012).

12 Richards, C. H. *et al.* The relationships between cellular components of the peritumoural inflammatory response, clinicopathological characteristics and survival in patients with primary operable colorectal cancer. *Br J Cancer* **106**, 2010-2015, doi:10.1038/bjc.2012.211 (2012).

13 Schmidt, M. *et al.* A comprehensive analysis of human gene expression profiles identifies stromal immunoglobulin kappa C as a compatible prognostic marker in human solid tumors. *Clin Cancer Res* **18**, 2695-2703, doi:10.1158/1078-0432.CCR-11-2210 (2012).

14 Iglesia, M. D. *et al.* Prognostic B-cell signatures using mRNA-seq in patients with subtype-specific breast and ovarian cancer. *Clin Cancer Res* **20**, 3818-3829, doi:10.1158/1078-0432.CCR-13-3368 (2014).

15 Yanni, G., Whelan, A., Feighery, C. & Bresnihan, B. Analysis of cell populations in rheumatoid arthritis synovial tissues. *Semin Arthritis Rheum* **21**, 393-399 (1992).

16 Pitzalis, C., Jones, G. W., Bombardieri, M. & Jones, S. A. Ectopic lymphoid-like structures in infection, cancer and autoimmunity. *Nat Rev Immunol* **14**, 447-462, doi:10.1038/nri3700 (2014).

17 Dieu-Nosjean, M. C. *et al.* Long-term survival for patients with non-small-cell lung cancer with intratumoral lymphoid structures. *J Clin Oncol* **26**, 4410-4417, doi:26/27/4410 [pii]
10.1200/JCO.2007.15.0284 (2008).

18 Martinet, L. *et al.* Human solid tumors contain high endothelial venules: association with T- and B-lymphocyte infiltration and favorable prognosis in breast cancer. *Cancer Res* **71**, 5678-5687, doi:0008-5472.CAN-11-0431 [pii]
10.1158/0008-5472.CAN-11-0431 (2011).

19 Coppola, D. *et al.* Unique ectopic lymph node-like structures present in human primary colorectal carcinoma are identified by immune gene array profiling. *Am J Pathol* **179**, 37-45, doi:S0002-9440(11)00320-8 [pii]
10.1016/j.ajpath.2011.03.007 (2011).

20 Clarke, B. *et al.* Intraepithelial T cells and prognosis in ovarian carcinoma: novel associations with stage, tumor type, and BRCA1 loss. *Mod Pathol* **22**, 393-402, doi:10.1038/modpathol.2008.191 (2009).

21 Lohr, M. *et al.* The prognostic relevance of tumour-infiltrating plasma cells and immunoglobulin kappa C indicates an important role of the humoral immune response in non-small cell lung cancer. *Cancer Lett* **333**, 222-228, doi:10.1016/j.canlet.2013.01.036 (2013).

22 Rangel-Moreno, J. *et al.* Omental milky spots develop in the absence of lymphoid tissue-inducer cells and support B and T cell responses to peritoneal antigens. *Immunity* **30**, 731-743, doi:10.1016/j.immuni.2009.03.014 (2009).

23 deLeeuw, R. J. *et al.* CD25 Identifies a Subset of CD4+FoxP3- TIL That Are Exhausted Yet Prognostically Favorable in Human Ovarian Cancer. *Cancer Immunol Res* **3**, 245-253, doi:10.1158/2326-6066.CIR-14-0146 (2015).

24 Darce, J. R., Arendt, B. K., Wu, X. & Jelinek, D. F. Regulated expression of BAFF-binding receptors during human B cell differentiation. *J Immunol* **179**, 7276-7286 (2007).

25 O'Connor, B. P. *et al.* BCMA is essential for the survival of long-lived bone marrow plasma cells. *J Exp Med* **199**, 91-98, doi:10.1084/jem.20031330 (2004).

26 Gentles, A. J. *et al.* The prognostic landscape of genes and infiltrating immune cells across human cancers. *Nat Med*, doi:10.1038/nm.3909 (2015).

27 Cerami, E. *et al.* The cBio cancer genomics portal: an open platform for exploring multidimensional cancer genomics data. *Cancer Discov* **2**, 401-404, doi:10.1158/2159-8290.CD-12-0095 (2012).

28 Kunkel, E. J. & Butcher, E. C. Plasma-cell homing. *Nat Rev Immunol* **3**, 822-829, doi:10.1038/nri1203 (2003).

29 Schumacher, T. N. & Schreiber, R. D. Neoantigens in cancer immunotherapy. *Science* **348**, 69-74, doi:10.1126/science.aaa4971 (2015).

30 Tothill, R. W. *et al.* Novel molecular subtypes of serous and endometrioid ovarian cancer linked to clinical outcome. *Clin Cancer Res* **14**, 5198-5208, doi:14/16/5198 [pii] 10.1158/1078-0432.CCR-08-0196 (2008).

31 George, J. *et al.* Nonequivalent gene expression and copy number alterations in high-grade serous ovarian cancers with BRCA1 and BRCA2 mutations. *Clin Cancer Res* **19**, 3474-3484, doi:10.1158/1078-0432.CCR-13-0066 (2013).

32 Bindea, G. *et al.* Spatiotemporal dynamics of intratumoral immune cells reveal the immune landscape in human cancer. *Immunity* **39**, 782-795, doi:S1074-7613(13)00437-8 [pii] 10.1016/j.immuni.2013.10.003 (2013).

33 Qin, Z. *et al.* B cells inhibit induction of T cell-dependent tumor immunity. *Nat Med* **4**, 627-630 (1998).

34 Olkhanud, P. B. *et al.* Tumor-evoked regulatory B cells promote breast cancer metastasis by converting resting CD4(+) T cells to T-regulatory cells. *Cancer Res* **71**, 3505-3515, doi:10.1158/0008-5472.CAN-10-4316 (2011).

35 Fillatreau, S. Regulatory plasma cells. *Curr Opin Pharmacol* **23**, 1-5, doi:10.1016/j.coph.2015.04.006 (2015).

36 Shalapour, S. *et al.* Immunosuppressive plasma cells impede T-cell-dependent immunogenic chemotherapy. *Nature* **521**, 94-98, doi:10.1038/nature14395 (2015).

37 Muehlinghaus, G. *et al.* Regulation of CXCR3 and CXCR4 expression during terminal differentiation of memory B cells into plasma cells. *Blood* **105**, 3965-3971, doi:10.1182/blood-2004-08-2992 (2005).

38 Lacotte, S. *et al.* Early differentiated CD138(high) MHCII+ IgG+ plasma cells express CXCR3 and localize into inflamed kidneys of lupus mice. *PLoS One* **8**, e58140, doi:10.1371/journal.pone.0058140 (2013).

39 Chihara, N. *et al.* Plasmablasts as migratory IgG-producing cells in the pathogenesis of neuromyelitis optica. *PLoS One* **8**, e83036, doi:10.1371/journal.pone.0083036 (2013).

40 Jiang, Y., Li, Y. & Zhu, B. T-cell exhaustion in the tumor microenvironment. *Cell Death Dis* **6**, e1792, doi:10.1038/cddis.2015.162 (2015).

41 Vidarsson, G., Dekkers, G. & Rispens, T. IgG subclasses and allotypes: from structure to effector functions. *Front Immunol* **5**, 520, doi:10.3389/fimmu.2014.00520 (2014).

42 Carmi, Y. *et al.* Allogeneic IgG combined with dendritic cell stimuli induce antitumour T-cell immunity. *Nature* **521**, 99-104, doi:10.1038/nature14424 (2015).

43 Germain, C. *et al.* Presence of B cells in tertiary lymphoid structures is associated with a protective immunity in patients with lung cancer. *Am J Respir Crit Care Med* **189**, 832-844, doi:10.1164/rccm.201309-1611OC (2014).

44 Yasuda, M. *et al.* Antigens recognized by IgG derived from tumor-infiltrating B lymphocytes in human lung cancer. *Anticancer Res* **26**, 3607-3611 (2006).

45 Kotlan, B. *et al.* Novel ganglioside antigen identified by B cells in human medullary breast carcinomas: the proof of principle concerning the tumor-infiltrating B lymphocytes. *J Immunol* **175**, 2278-2285 (2005).

46 Hansen, M. H., Nielsen, H. & Ditzel, H. J. The tumor-infiltrating B cell response in medullary breast cancer is oligoclonal and directed against the autoantigen actin exposed on the surface of apoptotic cancer cells. *Proc Natl Acad Sci U S A* **98**, 12659-12664, doi:10.1073/pnas.171460798 (2001).

47 Joyce, J. A. & Fearon, D. T. T cell exclusion, immune privilege, and the tumor microenvironment. *Science* **348**, 74-80, doi:10.1126/science.aaa6204 (2015).

48 Kanodia, S. *et al.* Expression of LIGHT/TNFSF14 combined with vaccination against human papillomavirus Type 16 E7 induces significant tumor regression. *Cancer Res* **70**, 3955-3964, doi:0008-5472.CAN-09-3773 [pii]
10.1158/0008-5472.CAN-09-3773.

49 Maldonado, L. *et al.* Intramuscular therapeutic vaccination targeting HPV16 induces T cell responses that localize in mucosal lesions. *Sci Transl Med* **6**, 221ra213, doi:10.1126/scitranslmed.3007323 (2014).

50 Lutz, E. R. *et al.* Immunotherapy converts nonimmunogenic pancreatic tumors into immunogenic foci of immune regulation. *Cancer Immunol Res* **2**, 616-631, doi:10.1158/2326-6066.CIR-14-0027 (2014).

Figure legends:

Fig. 1. *Six-color IHC reveals four types of lymphoid aggregate in HGSC and associations with TIL*. Antibodies to CD3 (green), CD8 (purple), CD20 (red), CD21 (blue), CD208 (black), and PNAd (brown) were used to visualize lymphoid aggregates in whole tumor sections from 30 HGSC cases. **A)** Type 1 aggregates contained CD8+ T cells, CD4+ T cells (detected as CD3+CD8- cells), CD20+ B cells, and CD208+ DCs. **B**) Type 2 aggregates contained CD8+ T cells, CD4+ T cells and CD20+ B cells in diffuse patterns with no clear follicles or T cell zones. **C**) Type 3 aggregates (TLS) contained B cell follicles with germinal centers (GC) distinguished by interdigitating networks of CD21+ fDCs. B cell follicles were adjacent to T cell zones containing primarily CD4+ T cells and CD208+ DCs, as well as CD8+ T cells. PNAd+ vessels were found in T cell zones and surrounding follicles. **D**) Type 4 aggregates contained CD20+ B cells and CD21+ fDCs without clear T cell zones and may represent milky spots. **E)** Densities of CD4+, CD8+ and CD20+ TIL in tumors in which TLS were present (n=7) or absent (n=23). **F)** Mean densities of CD4+, CD8+ and CD20+ TIL in 10 random fields versus 10 fields within 500 μm of a TLS center (n=7 cases). *P*-values refer to means that were compared using unpaired (E) or paired (F) *t* tests. Scale bars: A and D = 50 μm, B and C=100 μm.

Fig. 2. *Evidence of ongoing immune reactions within TLS in HGSC.* TLS were analyzed by multicolor IHC for various immune-related markers. **A)** Three-color stain for BCL-6 (brown), CD3 (green), and CD20 (red) showing BCL-6+ B cells and follicular helper T cells (Tfh) in a GC. **B)** Two-color stain for AID (brown) and CD20 (red) showing AID+ B cells in a GC. **C**) Three-color stain for CD38 (brown), CD79a (blue), and CD138 (red) showing dense stromal

infiltration by PCs (PC score = 3). **D**) False-colored image of PCs showing co-localization of CD38 (green) and CD138 (red) (merge = yellow). **E**) Example of a TLS surrounded by PCs. GC = germinal center. **F**) CD138+ cells (arrow) within a TLS-associated GC, possibly representing an early stage of PC differentiation. **G**) Average stromal density of PCs (on a scale of 0-3) in tumors without (n=23) and with (n=7) TLS. *P*-value, Mann-Whitney test. **H**) Association between stromal PC scores and the average density of CD4+, CD8+ and CD20+ TIL. *r* and *P* values refer to Spearmann's correlation. Scale bars: A, B, D = 50 μm; C = 100 μm; E, F = 200 μm.

Fig. 3. *Cell surface phenotypes and clonality of B-lineage cells in HGSC*. (**A-C**) Multicolor flow cytometry was used to analyze TIL from 12 disaggregated tumor samples. Data is color-coded as follows: *red* = naive B cells (IgD+, CD38-), *blue* = memory B cells (IgD- CD38-), and *green* = PCs (IgD-, CD38hi). **A**) Representative contour plot showing expression of IgD and CD38 on CD19+ cells. **B**) IgG expression on CD19+ cells. **C**) Expression levels (mean fluorescence intensity, MFI) of the indicated cell surface markers on CD19+ cells from a subset tumor samples. The same color-coding scheme is used as in panels A and B. **D**) Diversity and sharing of Ig V regions from PCs, memory B cells, and bulk tumor tissue from a representative HGSC case. The overall size of each pie indicates the relative number of unique productive IgG sequences observed in each sample. The size of each pie slice indicates the relative abundance of each VDJ rearrangement within a sample. VDJ rearrangements that were found in more than one sample are colored to show the pattern of sharing between samples. VDJ rearrangements that were found in only one sample are shown on a gray scale. Similar results were seen with two other HGSC cases.

Fig. 4. *Relationship between PCs, TIL subsets, and patient survival*. **A)** Venn diagram showing the inter-relationships between TIL subsets in the 172-case HGSC TMA. Colored circles indicate patient subgroups that were positive for the indicated TIL subsets: *blue* = CD8, *orange* = CD4, *pink* = CD20, *green* = PCs. Numbers indicate the proportion (%) of cases in each subgroup. **B)** Kaplan-Meyer analysis of disease-specific survival for six patient subgroups based on the indicated TIL patterns. *P*-values refer to log-rank tests between the indicated groups.

Fig. 5. *Gene expression analysis reveals a two-gene PC signature.* **A**) NanoString gene-expression analysis comparing Log_{10} average gene counts from tumors containing no PC infiltrates (n=4) to those with heavy PC infiltrates (n=3). Highlighted genes are those expressed at a greater than 10-fold differential between groups. **B**) Standardized microarray gene expression values (z-scores) for *IGJ* vs *TNFRSF17* from TCGA Affymetrix U133HT Genechip data showing three distinct patient subgroups (n=570). **C**) Standardized read-count data (fragments per kilobase per million reads; FPKM) for *IGJ* and *TNFRSF17* from the TCGA RNA-seq dataset (n=273). Data points are colored based on calls from microarray data (panel B). **D**) *IGHV*-region expression (FPKM) in TCGA cases exhibiting the *TNFRSF17*/*IGJ* PC signature, the *IGJ* B cell signature, or no B cell signature. The right panel shows an expanded view of *IGHV* regions from PC signature positive cases.

Fig.6. *The PC gene signature is associated with markers of active humoral and cellular immunity, patient survival, and CT antigen expression.* As in Figure 5, TCGA cases were stratified into three groups based on the expression of *IGJ* and *TNFRSF17*: *red* = no B cell

signature, *blue* = B cell signature, and *green* = PC signature. **A**) Expression of TLS-associated factors. **B**) Expression of chemokine ligands for CXCR3. **C**) Expression of PC survival factors. **D**) Expression of *CD8A*, an indicator of CD8+ TIL. **E)** Expression of *FOXP3*. **F**) Expression of cytotoxicity-associated gene products. For panels A-F, *P*-values refer to one-way ANOVA with Tukey *post hoc* comparison. *P<0.05, ***P<0.001, ****P<0.0001. **G**) Kaplan-Meier survival analysis of HGSC cases from the TCGA dataset (n = 570). **Log-rank tests between indicated groups: No B cells vs. PC *P* = 0.0086, B cells vs. PC *P*= 0.0241. **H)** TCGA RNA-seq normalized gene expression values for *IGJ* and *TNFRSF17* were overlaid with calls for above median levels of non-synonymous point mutations (n=219). *P*-value, chi-squared test. **I**) Analysis was performed as in panel A but overlaid with *BRCA1* alterations (including germline and somatic mutations and promotor methylation) and *BRCA2* mutations (germline and somatic) (n=316). *P*-value, chi-squared test. **J**) Average numbers of expressed CT antigens (TCGA microarray gene expression values >3 standard deviations above the mean) in cases with no B cell signature, the B cell signature, or the PC signature (n=570). *P*-value, one-way ANOVA with Tukey *post hoc* comparisons; ** *P* <0.01, ***P <0.0001.

Figures:

Figure 1

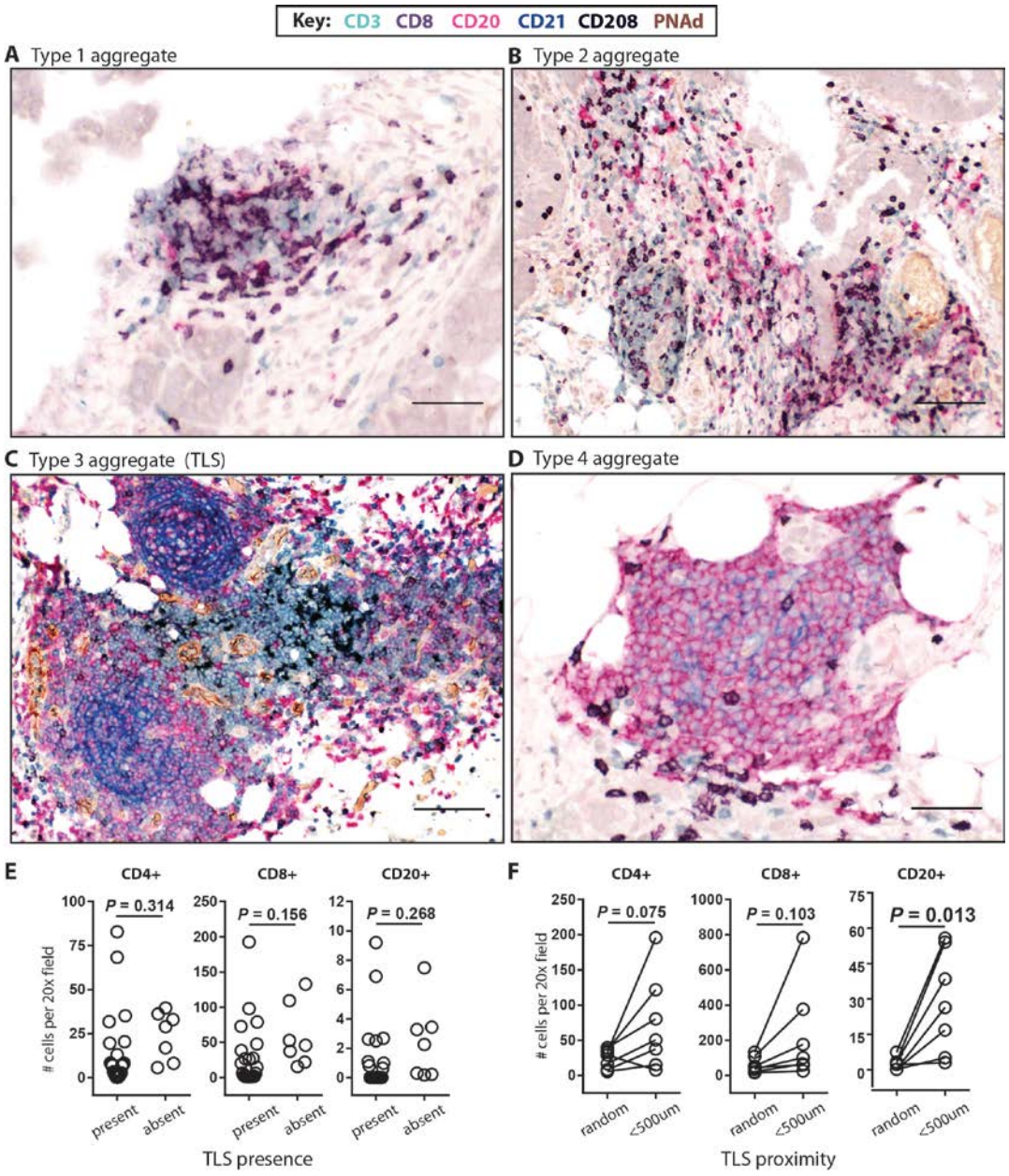

Figure 2

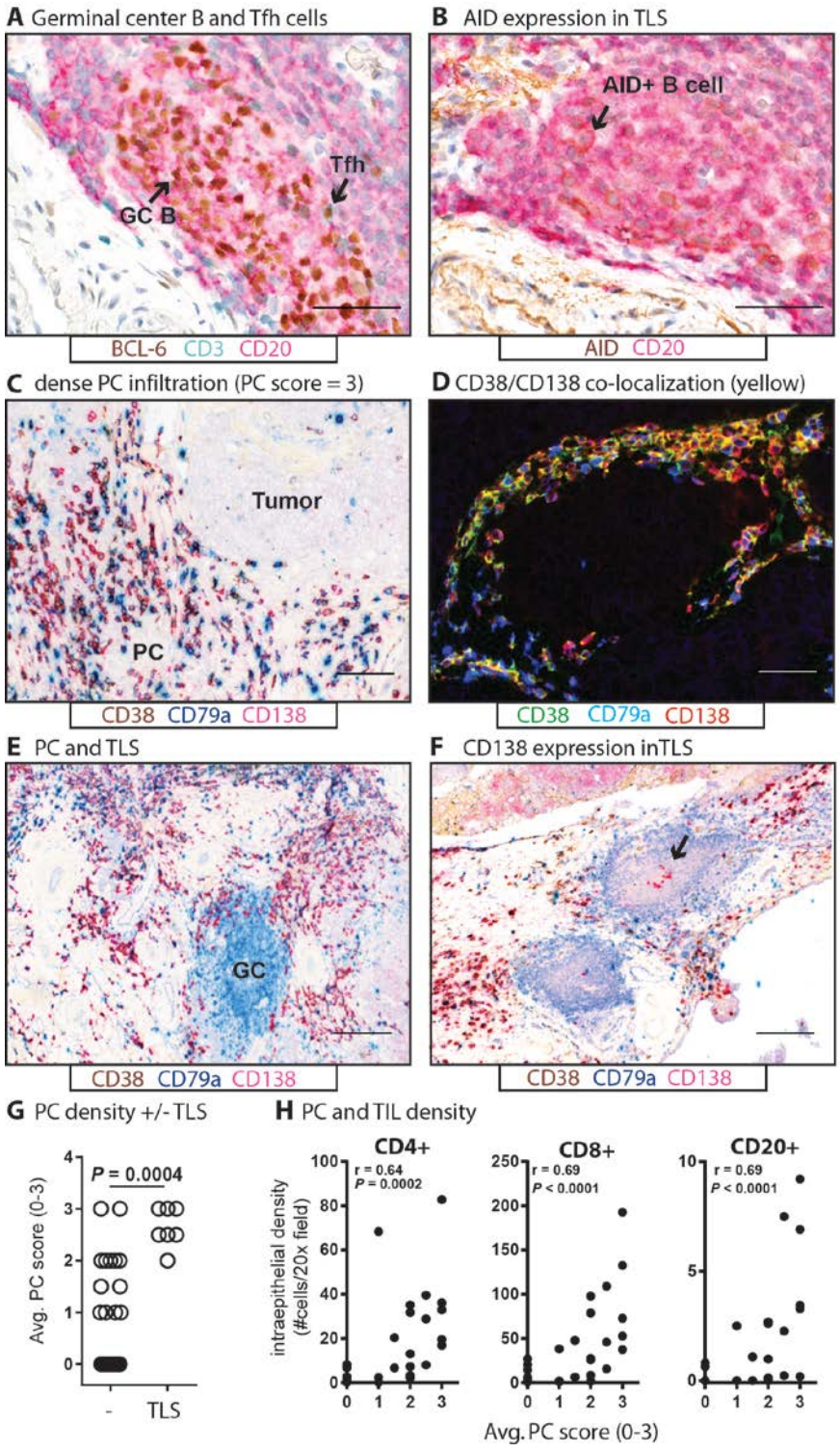
A Germinal center B and Tfh cells
GC B
Tfh
BCL-6 CD3 CD20
B AID expression in TLS
AID+ B cell
AID CD20
C dense PC infiltration (PC score = 3)
Tumor
PC
CD38 CD79a CD138
D CD38/CD138 co-localization (yellow)
CD38 CD79a CD138
E PC and TLS
GC
CD38 CD79a CD138
F CD138 expression inTLS
CD38 CD79a CD138
G PC density +/- TLS
P = 0.0004
Avg. PC score (0-3)
-
TLS
H PC and TIL density
CD4+
r = 0.64
P = 0.0002
CD8+
r = 0.69
P < 0.0001
CD20+
r = 0.69
P < 0.0001
intraepithelial density
(#cells/20x field)
Avg. PC score (0-3)

Figure 3

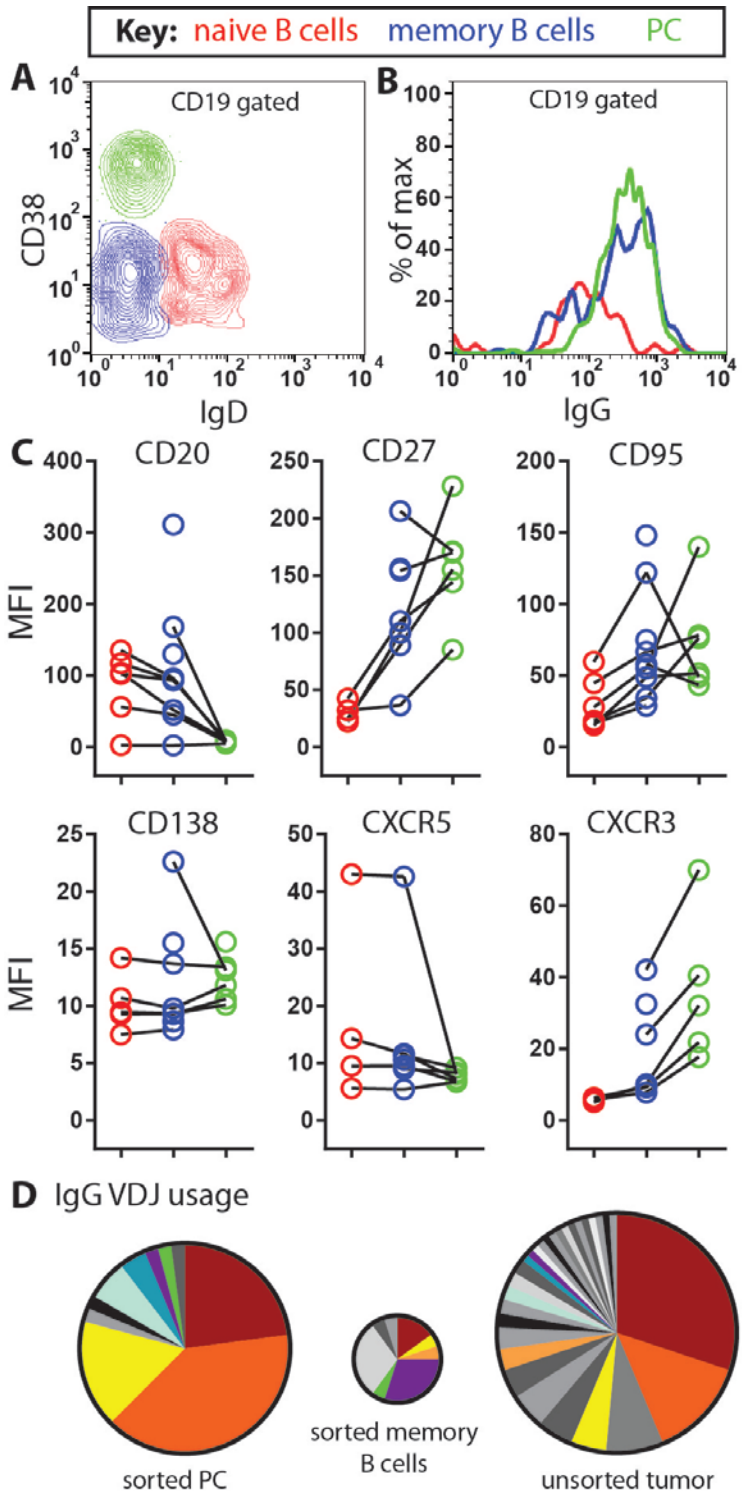
Key: naive B cells memory B cells PC
A
CD19 gated
CD38
IgD
B
CD19 gated
% of max
IgG
C
CD20
CD27
CD95
CD138
CXCR5
CXCR3
MFI
MFI
D IgG VDJ usage
sorted PC
sorted memory B cells
unsorted tumor

Figure 4

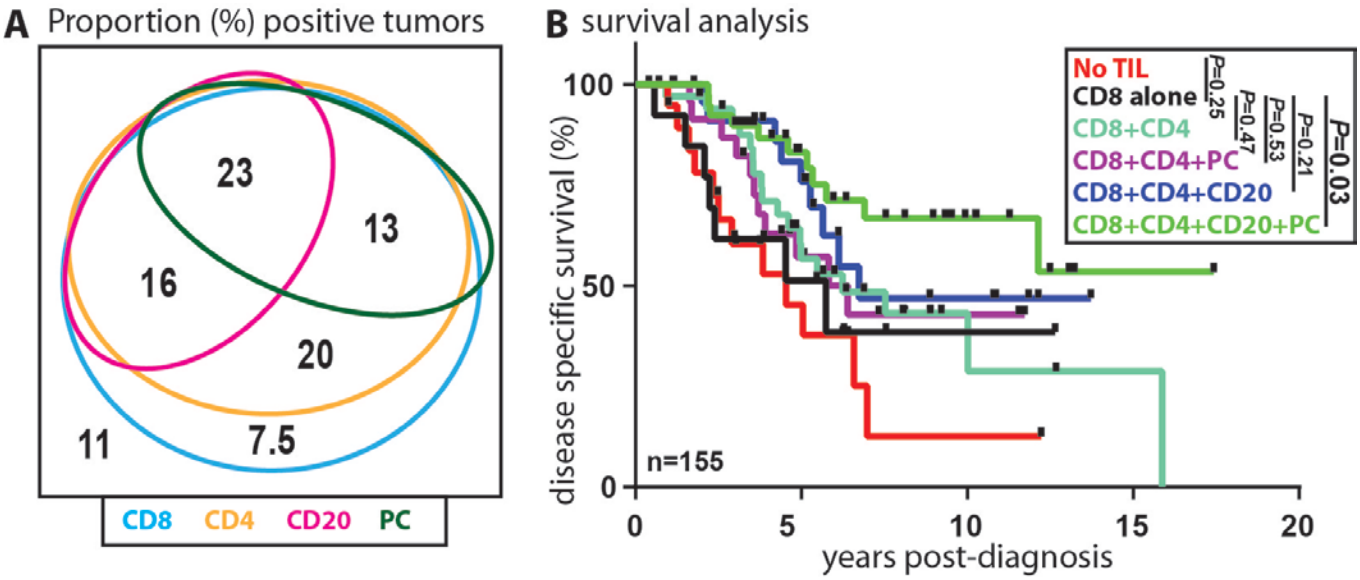
A Proportion (%) positive tumors
23
13
16
20
11
7.5
CD8
CD4
CD20
PC
B survival analysis
disease specific survival (%)
100
50
0
n=155
0
5
10
15
20
years post-diagnosis
No TIL
CD8 alone
CD8+CD4
CD8+CD4+PC
CD8+CD4+CD20
CD8+CD4+CD20+PC
P=0.25
P=0.47
P=0.53
P=0.21
P=0.03

Figure 5

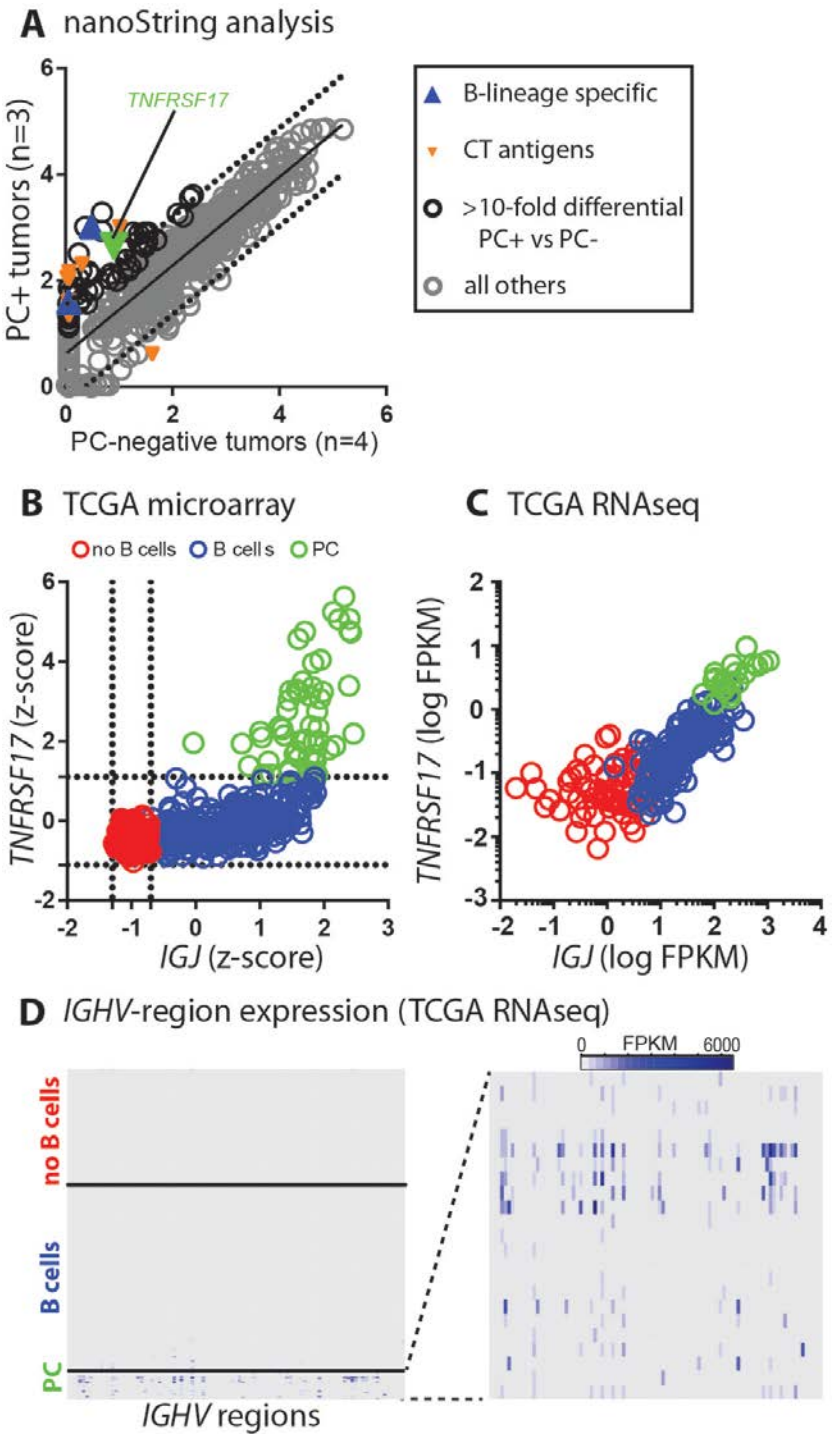
A nanoString analysis
TNFRSF17
PC+ tumors (n=3)
PC-negative tumors (n=4)
B-lineage specific
CT antigens
>10-fold differential PC+ vs PC-
all others
B TCGA microarray
no B cells
B cells
PC
TNFRSF17 (z-score)
IGJ (z-score)
C TCGA RNAseq
TNFRSF17 (log FPKM)
IGJ (log FPKM)
D IGHV-region expression (TCGA RNAseq)
FPKM
0
6000
no B cells
B cells
PC
IGHV regions

Figure 6

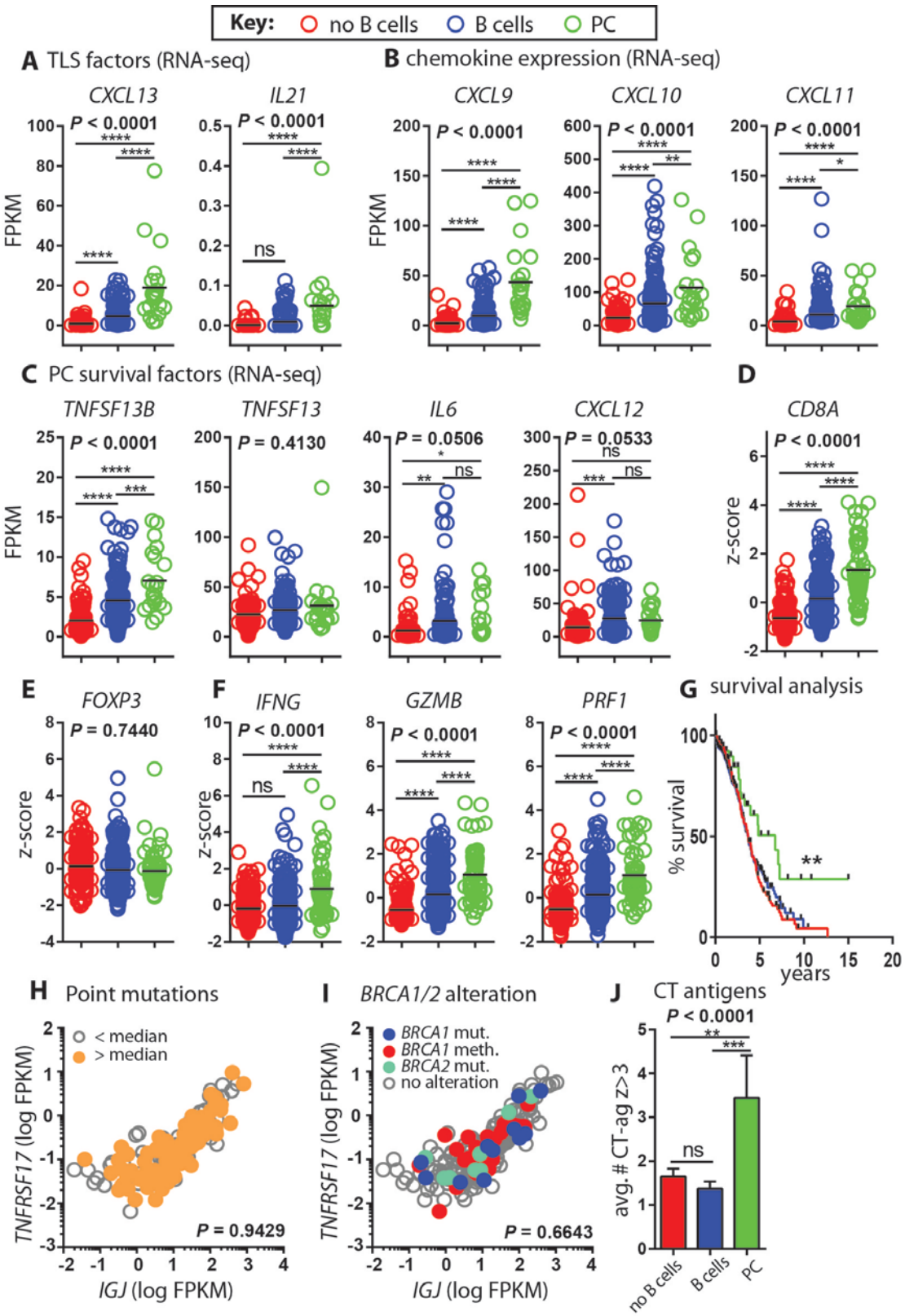
Key: no B cells B cells PC
A TLS factors (RNA-seq)
B chemokine expression (RNA-seq)
CXCL13
IL21
CXCL9
CXCL10
CXCL11
FPKM
P < 0.0001
P < 0.0001
P < 0.0001
P < 0.0001
P < 0.0001
ns
C PC survival factors (RNA-seq)
D
TNFSF13B
TNFSF13
IL6
CXCL12
CD8A
P < 0.0001
P = 0.4130
P = 0.0506
P = 0.0533
P < 0.0001
z-score
E
F
G survival analysis
FOXP3
IFNG
GZMB
PRF1
P = 0.7440
P < 0.0001
P < 0.0001
P < 0.0001
% survival
years
H Point mutations
I BRCA1/2 alteration
J CT antigens
< median
> median
BRCA1 mut.
BRCA1 meth.
BRCA2 mut.
no alteration
TNFRSF17 (log FPKM)
IGJ (log FPKM)
P = 0.9429
P = 0.6643
P < 0.0001
avg. # CT-ag z>3
no B cells
B cells
PC